TECHNICAL REPORT

NASA Research Grant NAG-1-279
University of Massachusetts Account # 5-28903
"Near Millimeter Wave Imaging/Multi-Beam Integrated Antennas"

Period Covered: October 1, 1985 — March 31, 1986
Principal Investigator: Professor K. Sigfrid Yngvesson
Co-Investigator: Associate Professor Daniel H. Schaubert

Department of Electrical and Computer Engineering
University of Massachusetts
Amherst, MA 01003

(NASA-CR-176989) NEAR MILLIMETER WAVE IMAGING/MULTI-BEAM INTEGRATED ANTENNAS Technical Report, 1 Oct. 1985 - 31 Mar. 1986 (Massachusetts Univ.) 71 p CSCL 20N
N86-30891 THRU N86-30893
Unclas
G3/32 43137

TECHNICAL REPORT

NASA Research Grant NAG-1-279
University of Massachusetts Account # 5-28903
"Near Millimeter Wave Imaging/Multi-Beam Integrated Antennas"

Period Covered:	October 1, 1985 — March 31, 1986
Principal Investigator:	Professor K. Sigfrid Yngvesson
Co-Investigator:	Associate Professor Daniel H. Schaubert

Department of Electrical and Computer Engineering
University of Massachusetts
Amherst, MA 01003

Table of Contents

N86-30892
D1
53P.

1. Theoretical Models of Single–Element LTSA Antenna Elements

18337
MK 149394

1.1 *Formulas for Z_o and λ'/λ_o of Slotlines*

The spectral domain computations for slotline guide wavelength and characteristic impedance that have been described in previous reports provide the basic parameters that are needed to calculate the radiation pattern of an LTSA antenna by using the half–plane Green's function and a stepped approximation to the LTSA structure. However, the spectral domain computations are somewhat time comsuming and not suitable for a CAD application. Therefore, the results of several computations have been fitted by formulas that are readily evaluated on a calculator or computer. These formulas appear in the revised manuscript (Appendix A) that has been accepted for publication in the IEEE Transactions on Microwave Theory and Techniques.

1.2 *Effects of E–Plane Truncation*

It has been observed and reported in the previous report that the E–plane beamwidth is quite sensitive to the antenna half–height D (see Fig. 1.1). We have measured many antennas on air and higher ϵ_r substrates, and have substantiated that the effect becomes important for D in the range of 2–3 λ_o ($w_o = 0.5\ \lambda_o$). During this reporting period, we have continued to measure antennas and have attempted to predict the truncation effect by three different methods. These are described below. A typical example of the truncation effect was presented in the last report and is repeated as Figure 1.2 for convenience.

1.2.1 *GTD Analysis*

Scattering from the upper and lower edges of the antenna in Figure 1 can be evaluated by using GTD. However, GTD is based on ray optics so the angular region over which the scattering affects the radiation pattern does not include the main beam. This is illustrated in Figure 1.3 with two typical rays. Ray 1 affects the far out sidelobe region, whereas ray 2 represents the closest that any edge diffracted ray can approach to boresight. For all cases in Figure 1.2, the cone of diffracted rays lies well outside of the 3–dB beamwidth of the antenna.

Tip diffracted rays from points A and B could contribute to the main–beam region, but the fields from these rays should be quite small because i) tip diffraction is weaker than edge diffraction which is weaker than the direct field, and ii) the polarization of interest requires that we consider slope diffraction. Unfortunately, a slope diffraction coefficient for tips has not been determined, so we cannot substantiate these statements with numerical results, but we believe them to be correct.

Other multiple diffraction rays that involve the edge C could affect the main beam, but we expect their effect to be small since they come primarily from the backward radiation, which is 10 dB or more below the main beam.

1.2.2 *Finite Strip Green's Function*

The use of the half–plane Green's function is a key step in the success of our method in predicting the radiation pattern of antennas with $D \longrightarrow \infty$. Therefore, we have investigated the use of a Green's function for a finite width strip of conductor. This Green's function cannot be obtained in a simple form. Attempts to obtain it by mode matching, which works well for the half–plane, lead to a system of coupled integral equations that

must be solved for a large number of modes. We have not discovered an efficient means of obtaining the required Green's function.

1.2.3 *Moment Method for Air Dielectric*

For air dielectric LTSAs, the moment method can be employed to calculate the current distribution on the conducting plates that form the antenna. We have modified a version of Newman's computer code from Ohio State University to calculate the current distribution and radiation patterns on antennas comprised of rectangular plates (see Fig. 1.4). The use of rectangular instead of quadralateral plates simplifies the analysis because a rectangular grid can be used for the subdomains and current expansion functions. The current expansion functions are piecewise sinusoids along the direction of current flow and one cosine on a pedestal in the direction transverse to current flow. Two orthogonal components of current are included in the analysis. A simplified feed model comprising an infinitesimal electric current element in space is used to provide an incident field on the antenna. This model does not permit current to flow from one plate to the other, but the radiation patterns of strip dipoles (Figs. 1.5 and 1.6) agree quite well with known results. Also, the code accurately predicts the radar cross section of a flat plate (Figs. 1.7 and 1.8).

Measured and computed patterns for three cases do not show good agreement. The results for an antenna of length $L = 3\ \lambda_o$ are presented in Figures 1.9 and 1.10. The computed results in Figure 1.10 use a wire loop feed attached perpendicular to the plates at a distance of $0.05\ \lambda_o$ from the edges. This feed model permits current to flow from one plate to the other, but the computed patterns are nearly identical to those obtained

with the simpler current element. The curves labelled AFM are obtained with our half–plane Green's function method and the curves a, b, and c are obtained by the moment method with increasing number of segments on each plate. It appears that 5–6 segments per wavelength is adequate for convergence, but the computed E–plane beamwidth is 38° versus a measured value of 29°. Although this is an improvement over the Green's function prediction for $D \longrightarrow \infty$, it is still not acceptable and the moment solution often is no better than the Green's function prediction.

Measured patterns for L/λ_o of 4.8 and 5.2 are shown for various values of H in Figures 1.11 and 1.12. For $L/\lambda_o = 4.8$ and $H/\lambda_o = 1.0$, the measured beamwidths are 29° in the E–plane and 52° in the H–plane. The moment method predicts 44° and 60° for these and the $D \longrightarrow \infty$ Green's function predicts 42° and 49° (see Fig. 1.13). The moment method patterns for $L/\lambda_o = 5.16$ and $H/\lambda_o = 0.9$ and 0.75 are shown in Figure 1.14. The E–plane beamwidth prediction for $H/\lambda_o = 0.9$ is 35° whereas the measured value in Figure 1.12 is 25°. The measured H–plane is asymmetric due to the mount that was used, so these data are suspect. A comparison of the moment method predictions (MOM) and those of the $D \longrightarrow \infty$ Green's function method (AFM) is shown in Figure 1.15. The two methods agree quite well in the E–plane, but they differ somewhat in the H–plane.

We will continue to evaluate the moment method results and to measure more antennas in order to identify the key parameters that control the performance of the LTSA.

2. Coupling Effects in LTSA Arrays

2.1. *Review of Earlier Work on LTSA Array Coupling Effects*

Coupling effects in LTSA arrays were studied previously, in X–band scaled models as well as in 94 GHz arrays, and the results of these experiments were reported in the previous technical report, Appendix VIII, "A 94 Ghz Imaging Array Using Slot Line Radiators", comprising a Ph.D. Thesis by Thomas L. Korzeniowski. LTSA arrays with two different spacings, i.e. 7.9 mm and 5.0 mm, were investigated at 94 GHz. For both spacings, data were obtained for hexagonal (7 element) and square (9 element) configurations. A scaled model model of the 7.9 mm array was also fabricated, which scaled to about 10 GHz. The results may be summarized as follows:

- ⋆ In terms of impedance measurements, it was shown that the mutual impedance was negligible in the case of both arrays used at 94 GHz (model measurements performed at X–band). Mutual impedance became measurable only when the spacing was less than about one wavelength (the two spacings used at 94 GHz correspond to 2.2 and 1.6 wavelengths, respectively).

- ⋆ For the arrays with 7.9 mm spacing, beamwidths for elements on the central substrate were essentially unchanged in the H–plane, and considerably narrower in the E–plane, compared with a single element with the same dimensions. E–plane beam–widths were about the same on the outer substrate as on the central substrate, while the H–plane beam had a slight shoulder at about the –6 dB level on one side of the beam. It is interesting to note that the beam–shapes and beamwidths of all three elements on the central substrate were almost identical, although with some E–plane narrowing

compared with a single element. The above trends were found to occur for both the hexagonal and the square configurations.

* For the arrays with 5.0 mm spacing, E–plane beamwidths again narrowed consistently, but somewhat less than for the larger spacing. H–plane beam–shape was affected so that it became double–peaked for elements on the central substrate. The beamwidths in the H–plane were essentially unchanged for all array positions, however, compared with those of a single element.

* From the above data, we can conclude that the E–plane beamwidth is primarily determined by coupling to the other elements on the same substrate, while the H–plane beamwidth is changed only slightly. The H–plane beam–shape, on the other hand, is affected by the presence or absence of neighboring substrates in the H–plane.

Coupling effects were also studied in a 5 x 5 array of **CWSA** elements, in work done during Prof. Yngvesson's sabbatical visit to Chalmers University of Technology, see Appendix VI of the previous technical report for this grant. The antenna elements used in this case were shorter, and were matched to a smaller f–number reflector (f–#=1.0). Beams on the three central substrates have almost identical –10dB beamwidths in the E–plane, with only small variations (less than 1 dB) in individual beam–shapes. The E–plane beams on the "edge" elements (with respect to the E–plane direction) are skewed away from the center of one array. The H–plane beamwidths are somewhat wider than the E–plane ones, but are consistently the same, again excepting only the elements on the edge substrate (with respect to the H–plane direction), which have a –5 dB shoulder on the side of the beam away from the center. If one is willing to accept an extra row of "dummy" elements along the edges, then all inside elements have beam–widths which are acceptably similar

and symmetric. In many applications, the edge element patterns would also be acceptable. For convenience, we show this data in Figure 2.1.

The previous studies thus have shown the feasibility of constructing arrays with beam patterns for illumination of a reflector antenna with f–# of either 1.9 or 1.0. In both cases, the actual angular spacing between beams from adjacent elements when the arrays were used with the reflector antenna, was about one 3 dB beamwidth. Since it is important to determine what the limit on the beam–spacing is, and also to assess the effects of mutual coupling which do occur, we have continued to study the mutual coupling effects, and have chosen an LTSA–array with even smaller spacing (3.0 mm), so that the coupling effects would be clearly distinguishable. The new results are reported below.

2.2. *One Substrate, 1–4 elements in an "E–plane–array, 3 mm Spacing"*

The dimensions of a typical LTSA array used in this work are defined in Figure 2.2. Radiation patterns at 94 GHz were recorded for 1, 2, 3 and 4 elements on a single substrate, see Figure 2.3. In these experiments, a diode detector was soldered on one element at a time, while all other elements were left either open–circuited or shorted. We first discuss the open–circuited case. E–plane patterns show the expected symmetry. The largest distortion occurs for the two–element array, where a prominent shoulder appears at the –8 dB level on the side away from the center. For 3 or 4 elements, substantial shoulders are also found. The H–plane patterns tend to narrow for the edge elements, and widen for inner elements. Beam width, beam efficiency, and directivity data are given in Table 1. The inner elements of the four–element array, show a decreased directivity by more than 2 dB, compared with a single element. For all other elements, variations in directivity

by only about + −1 dB occur about the average, and all of these elements show a higher directivity than that of a single element. In summary, while quite large distortions occur in the patterns, a main beam remains. Only about + − 1 dB variation in directivity for all except the inner two elements, which show a decreased directivity of about 3 dB with respect to the average of all other elements.

The effect of changing the termination of the elements which were not being measured from an open circuit to either a short or the load represented by an un–biased diode, was also investigated. Directivities changed by amounts ranging from 0.5 to 1.5 dB, showing that waves on neighboring elements have a major influence on the radiation pattern being measured for a particular element, see Table 1. Radiation patterns with unused elements terminated with a diode are shown in Figures 2.4 and 2.5. They show a general similarity to the radiation patterns measured when unused elements are left open–circuited, shown in Figure 2.3.

It was of interest to investigate whether the direction of the main beam was being influenced by the coupling to neighboring elements. Figure 2.6a shows expanded radiation patterns in the E–plane of two elements on a substrate, with care being taken to use the same angular reference position for the two element patterns. As can be seen, there is a small (degrees) shift of the two beams with respect to each other. The expected shift of the beams due to geometric effects because of the finite distance to the source is much smaller than the measured shift. We therefore conclude that the shift in direction of the main beams is primarily due to coupling between the two elements. The H–plane patterns of the same two elements do not show any shift, as expected, see Figure 2.6b.

2.3. *Single Elements on Three Parallel Substrates, at Spacings of 3, 5, and 8 mm, "H-Plane Array"*

Single elements with the same dimensions were fabricated on three different substrates, and the effect of varying the spacing of the substrates was investigated. Spacings of 3, 5, and 8 mm were used. Data for these arrays, as well as for a single element on a single substrate, are compared in Table 2 and in Figure 2.7. Even at a substrate distance of 8 mm, these patterns show a narrowing of the beamwidths in both the E- and the H-plane, and directivities of 16–17 dB, compared with 12 dB directivity for a single element on a single substrate. These fairly drastic effects for the elements used in the present investigation should be compared with the much smaller effects evidenced in the arrays with 7.9 mm spacing which we reported earlier. The present elements have an opening angle which is one half of the one we used earlier, and this apparently results in much larger coupling between elements which are positioned in an H-plane array configuration. In order to further substantiate this conclusion, one needs to measure an array at different substrate separation. Interestingly, the arrays with the two smaller spacings show wider beams instead. They also have quite severely distorted beam shapes, and lower directivities than the 8 mm array, although only the center element of the 3 mm array has a directivity less than that of a single element on a single substrate. The directivity has been plotted versus substrate separation in Figure 2.8. The symmetry of the position of the element in the array is generally quite well reflected in the symmetry of its radiation pattern.

2.4. *Seven-Element Array on Three Parallel Substrates*

In the experiments described above, coupling effects were investigated between one-

dimensional arrays of elements arranged either in the E–plane or in the H–plane. The one–dimensional arrangement thus allows separation of coupling in the two planes. We also looked at the more complicated case of a two–dimensional array, specifically consisting of three–element arrays on two outer substrates and a four–element array on the central substrate. Selected radiation patterns for an element spacing on the substrates of 3 mm, and a substrate separation of 5 mm, are shown in Figure 2.9. The beams are only slightly more distorted in these cases. When the spacings between substrates were decreased to 3 mm, much more severe distortions were seen, and most of the directional character of the beams disappeared.

2.5. *Endfire Four–Element E–Plane Phased Array*

A simple E–plane array consisting of four elements on a substrate was constructed, and a slot–line power–splitter was designed to feed this array with equal phase for all elements. Despite the somewhat distorted element patterns (see Figure 2.10.) The array produces a beam with high directivity in the E–plane, and the nearest side–lobe at the –13 to –15 dB level.

3. Publications Based on Work on the Grant During the Period Covered by this Report

3.1 *Publications which Appeared in Journals*

★ "Endfire Tapered Slot Antennas on Dielectric Substrates", by K. Sigfrid Yngvesson, Daniel H. Schaubert, Thomas L. Korzeniowski, Erik L. Kollberg, Thomas Thungren and Joakim F. Johansson, IEEE Trans. Antennas and Prop., AP-33, 1392—1400 (Dec. 1985) (See Appendix C).

★ "Limitations of Microwave and Millimeter Wave Mixers Due to Excess Noise", by Gamal M. Hegazi, A. Jelenski, and K. Sigfrid Yngvesson, IEEE Trans. Microw. Theory Techn., MTT-33, 1404—1409 (Dec. 1985). The work published in this paper was supported by the NASA Langley Research Center grant in its initial phase (to early 1985) (See Appendix E).

3.2 *Ph.D. Thesis*

★ "Optimization of Low-Noise Millimeter Wave Receiver Front-Ends", by Gamal Mahmoud Hegazi, May 1986 (See Appendix B). The initial work for this Ph.D. thesis was supported by NASA Langley Research Center on this grant. Since early 1985 the work was supported by an industrial sponsor.

3.3 *Publications Accepted in Journals*

★ "Characterisitic Impedance of a Wide Slotline on Low-Permittivity Substrates", R. Janaswamy and D.H. Schaubert, a revised and expanded version of this paper will appear in IEEE Trans. Microw. Theory and Techn., August 1986 (See Appendix A).

* "Analysis of the TEM Mode Linearly Tapered Slot Antenna", R. Janaswamy, D.H. Schaubert and D.M. Pozar, has been accepted by Radio Science.

* "A New Integrated Slot Element Feed Array for Multi-Beam Systems", by K. Sigfrid Yngvesson, Joakim F. Johansson, and Erik L. Kollberg, Accepted for the November 1986 issue of the IEEE Trans. Antennas Propag.

3.4. *Papers Presented at Conferences and Published in Proceedings*

* "Model Experiments with Slot Antenna Arrays for Imaging", by J.F. Johansson, K.S. Yngvesson, and E.L. Kollberg, Presented at the SPIE Conference on Submillimeter Spectroscopy, Cannes, France, Dec. 1985 (See Appendix VI of the previous report on this grant).

* "Millimeter Wave Imaging with an Endfire Receptor Array", by K.S. Yngvesson, J. Johansson and E.L. Kollberg, Presented at the 10th Intern. Conf. on Infrared and Millimeter Waves, Orlando, Florida, Dec. 1985 (See Appendix IV of the previous report on this grant).

* "Imaging Front-End Systems for Millimeter Waves and Submillimeter Waves", by K.S. Yngvesson, Presented at the SPIE Conference on Submillimeter Spectroscopy, Cannes, France, Dec. 1985 (See Appendix V of the previous report on this grant).

Table 1. Data for elements in an array on one substrate.

# of Elem. in Array	Element # Pos.	Termin. Unused Elems.	Plane	3dB BW	10dB BW	-10dB Beam-eff. % E/H	-10dB Beam-eff. % Total	Directivity (dB)
1	1	N.A.	E	23.4	50.4	29.73	23.07	12.14
			H	24.3	37.8	17.81		
2	1	Open	E	15.3	43.2	29.93	25.01	15.13
			H	16.2	30.6	20.5		
	2	Open	E	14.4	42.3	30.8	30.73	15.5
			H	21.6	31.5	30.64		
2	1	Short	E	12.6	41.4	20.58	19.15	13.64
			H	20.7	30.6	17.78		
	2	Short	E	13.5	41.4	20.68	19.27	13.43
			H	21.6	30.6	18.02		
3	1	Open	E	18.9	39.6	22.74	23.62	13.84
			H	22.5	31.5	24.71		
	2	Open	E	14.4	29.8	18	21.56	13.81
			H	24.3	36	23.73		
	3	Open	E	19.8	41.4	23.56	24.94	13.89
			H	22.5	31.5	26.84		
3	1	Short	E	18	45.9	25.1	23.98	14.05
			H	20.7	32.4	22.72		
	2	Short	E	13.5	26.1	8.32	13.71	12.81
			H	23.4	32.4	19.3		
	3	Short	E	18	39.6	24.04	23.04	14.07
			H	18	32.4	21.84		
4	1	Open	E	21.6	51.3	33.85	31.07	13.92
			H	20.7	34.2	27.25		
	2	Open	E	19.8	35.1	8.05	11.99	9.85
			H	23.4	47.7	17.17		
	3	Open		21.6	36.9	8.86	13.32	9.56
			H	30.6	43.2	18.6		

Table 1, Continued

# of Elem. in Array	Element # Pos.	Termin. Unused Elems.	Plane	3dB BW	10dB BW	-10dB Beam-eff. % E/H	-10dB Beam-eff. % Total	Directivity (dB)
4	1	Short	E H	19.8 22.5	59.4 55.8	24.62 49.92	34.08	13.03
	2	Short	E H	20.7 23.4	37.8 46.8	10 9.53	9.74	9.04
	3	Short	E H	21.6 30.6	38.7 44.1	12.71 13.61	13.19	8.84
	4	Short	E H	19.8 26.1	60.3 54	29.4 58.34	39.36	12.92
2	1	Diode	E H	15.3 20.7	30.6 31.5	25.19 25.41	25.32	15.45
	2	Diode	E H	17.1 20.7	40.5 31.5	30.32 38.5	33.52	15.51
3	1	Diode	E H	15.3 22.5	41.4 33.3	24.21 21.92	23.0	13.82
	2	Diode	E H	14.4 19.8	26.1 32.4	15.95 25.83	20.66	14.89
	3	Diode	E H	18 20.7	39.6 33.3	37.74 36.94	31.73	15.24
4 (Phased Array)	N.A.	N.A.	E H	12.15 25.65	20.25 38.7	18.19 40.21	32.74	15.91

Table 2. Data for elements in an H–plane array on three substrates, one element on each substrate.

Substrate Spacing	Element Position	Plane	3 dB B.W.	10 dB B.W.	-10dB E/H	B.E. % Total	Directivity (dB)
3 mm	Top	E	28.8	45.9	39.42	36.48	12.73
	Left	H	32.4	45.9	34.28		
	Center	E	30.6	67.5	31.57	36.25	9.79
	Center	H	47.1	60.3	41.37		
	Bottom	E	22.5	48.6	35.97	50.61	13.06
	Right	H	35.1	54.9	61.15		
5 mm	Top	E	34.2	51.3	42.35	42.17	13.38
	Left	H	24.3	40.5	41.88		
	Center	E	17.1	60.3	50.62	47.72	13.16
	Center	H	34.2	44.1	44.89		
	Bottom	E	18	49.5	48.27	53.0	15.8
	Right	H	13.5	43.2	58.38		
8 mm	Top	E	26.1	42.75	51.88	47.73	15.72
	Left	H	15.3	37.37	40.96		
	Center	E	18	42.75	52.93	48.71	17.15
	Center	H	18.9	30.15	43.78		
	Bottom	E	20.25	37.8	46.43	38.5	16.13
	Right	H	15.75	31.05	31.82		

Figure Captions

Figure 1.1. LTSA with finite half-height D.

Figure 1.2. Measured patterns of LTSA on $\epsilon_4 = 2.22$ substrate. $L/\lambda_o = 3.4$, $2\gamma = 10^o$, $d/\lambda_o = 0.014$.

Figure 1.3. Edge diffracted ray cones for finite D antenna.

Figure 1.4. Antenna geometry for moment method analysis and experiments.

Figure 1.5. Strip dipole test case of moment solution; (a) radiation pattern and (b) current distribution.

Figure 1.6. Strip vee dipole test case.

Figure 1.7. Test case for radar cross section of $1\lambda_o \times 1\lambda_o$ plate.

Figure 1.8. Test case for radar corss section of $0.6\lambda_o \times 0.6\lambda_o$ plate.

Figure 1.9. Measured patterns for $L/\lambda_o = 3$, $H/\lambda_o = 0.75$; (a) E-plane and (b) H-plane.

Figure 1.10. Computed patterns for antenna in Figure 9.

Figure 1.11. Measured patterns for $L/\lambda_o = 4.8, \gamma = 5.9^o$; (a) $H/\lambda_o = 2.1$, (b) $H/\lambda_o = 1.33$, (c) $H/\lambda_o = 1.0$.

Figure 1.12. Measured patterns for $L/\lambda_o = 5.2$, $\gamma = 7^o$; (a) $H/\lambda_o = 2.46$, (b) $H/\lambda_o = 1.5$, (c) $H/\lambda_o = 0.9$.

Figure 1.13. Calculated patterns for $L/\lambda_o = 4.8$, $\gamma = 5.9^o$; (a) moment method, $H/\lambda_o = 1.0$ and (b) Green's function method, $D \longrightarrow \infty$.

Figure 1.14. Patterns calculated by moment method, $L/\lambda_o = 5.16$, $\gamma = 7^o$, $H/\lambda_o = 0.9$ and 0.75.

Figure 1.15. Comparison of patterns calculated by using moment method and Greens function method ($D \longrightarrow \infty$).

Figure 2.1. Radiation patterns of a 5 x 5 element CWSA array, measured at 31 GHz. The element spacing was 13 mm in both planes. (a) E-plane (b) H-plane.

Figure 2.2. Substrate with three LTSA elements.

Figure 2.3. Radiation patterns of elements in arrays with (from left to right) 1, 2, 3, and 4 LTSA elements on a single substrate, measured at 94 GHz. Position of pattern in the diagram indicates the position of the element which was measured. All other elements were left open–circuited. (a) E–plane patterns (b) H–plane patterns.

Figure 2.4. Radiation patterns of elements in an array with two elements, both terminated with diodes.

Figure 2.5. Radiation patterns of elements in an array with three elements, all terminated with diodes.

Figure 2.6. Radiation patterns with expanded scale for elements in an array of two elements, terminated in diodes. (a) E–plane (b) H–plane.

Figure 2.7. Radiation patterns for elements in an array consisting of three substrates, each with a single LTSA element. Spacings between substrates are marked. (a) E–plane (b) H–plane.

Figure 2.8. Directivity versus substrate separation for the array elements of Figure 2.7.

Figure 2.9. Radiation patterns of selected elements in a ten–element two–dimensional array. The location of the element measured is indicated schematically.

Figure 2.10. (a) Radiation pattern of a single element. (b) Radiation patterns of a four–element E–plane endfire phased array. Element spacing is 3 mm.

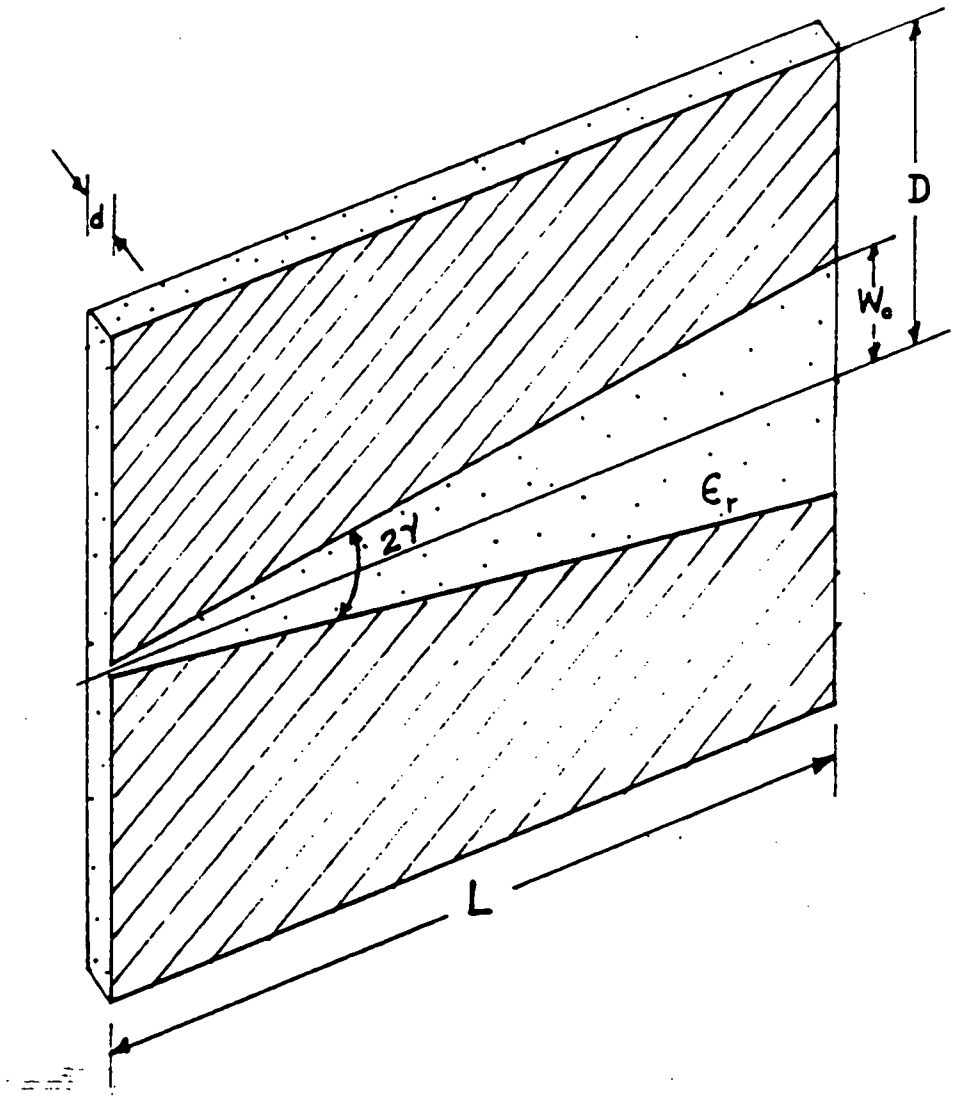

Fig. 1.1

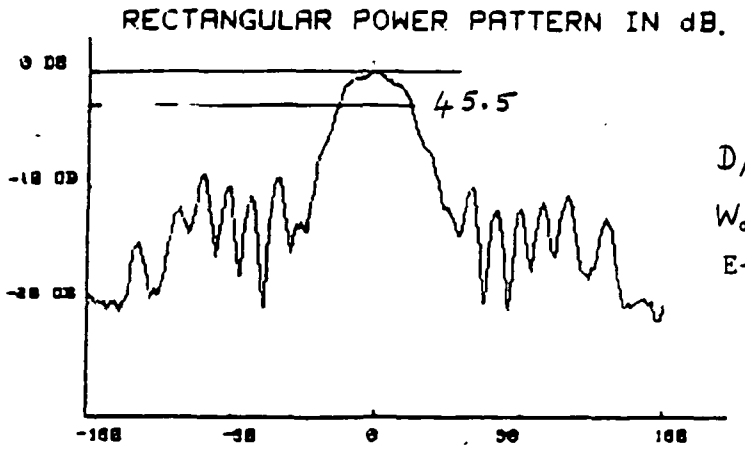
RECTANGULAR POWER PATTERN IN dB.
45.5
D/λ₀ = 2.4
W₀/D = 0.11
E-PLANE

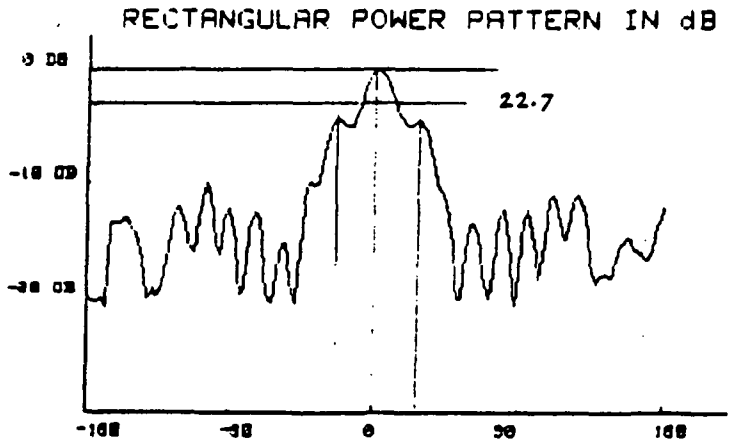
RECTANGULAR POWER PATTERN IN dB
22.7
D / λ₀ = 1.6
W₀/D = 0.17
E-PLANE

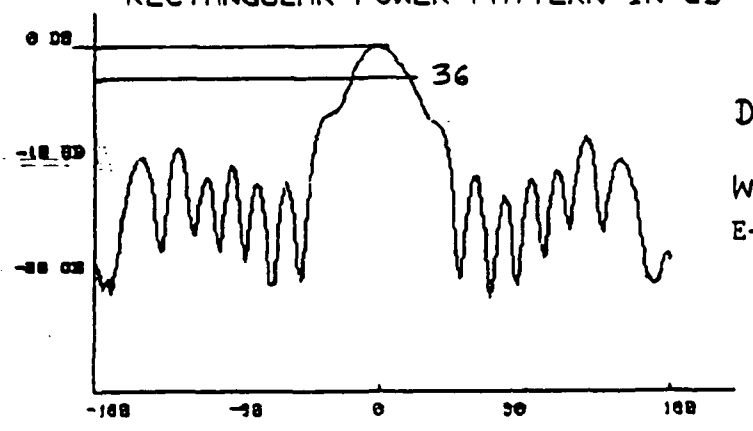
RECTANGULAR POWER PATTERN IN dB
36
D/λ₀ = 0.8
W₀/D = 0.33
E-PLANE

Fig. 1.2

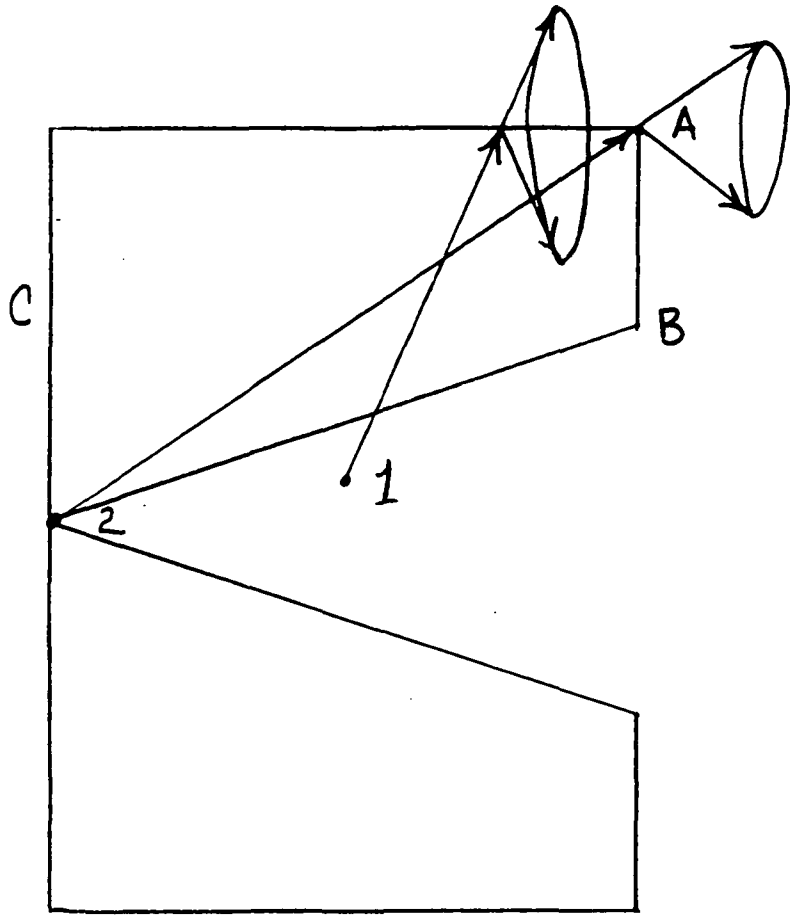

Fig. 1.3

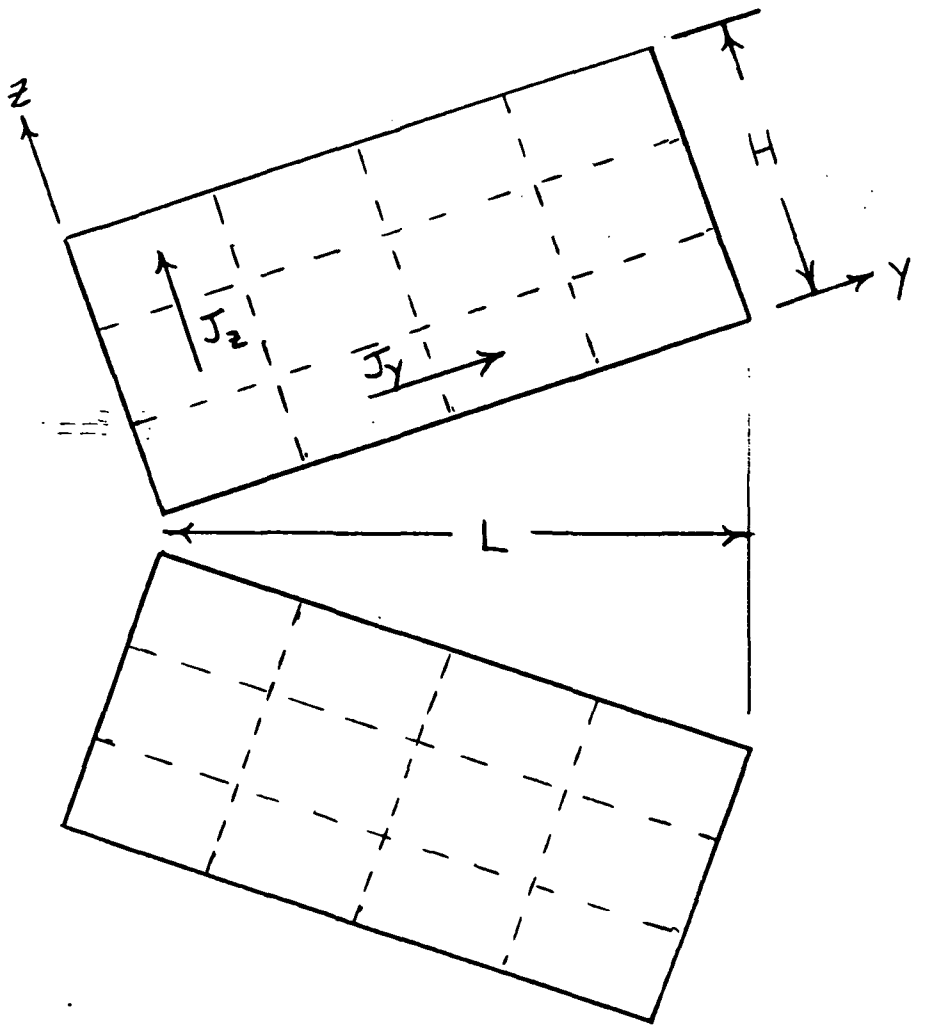

Fig. 1.4

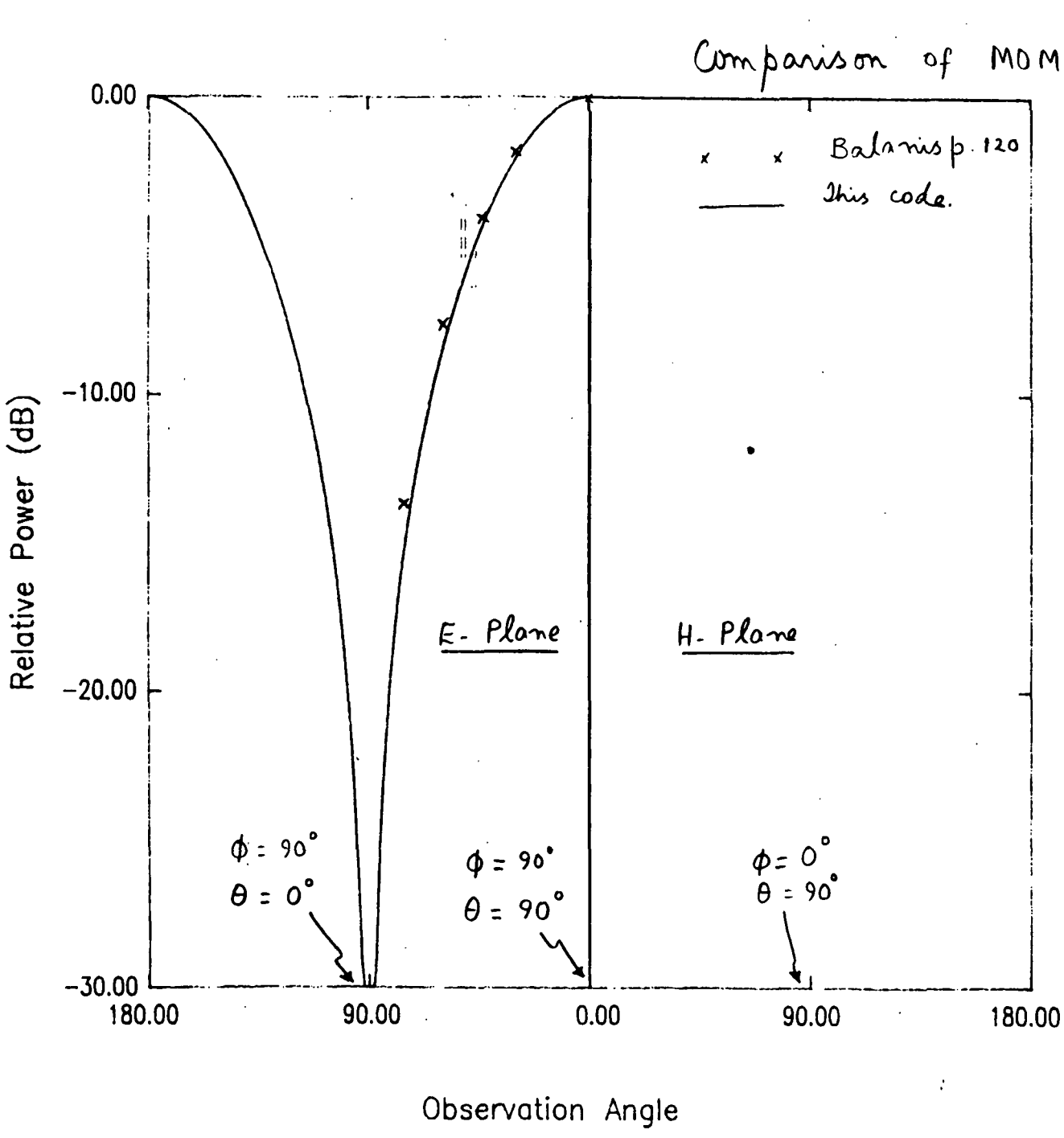

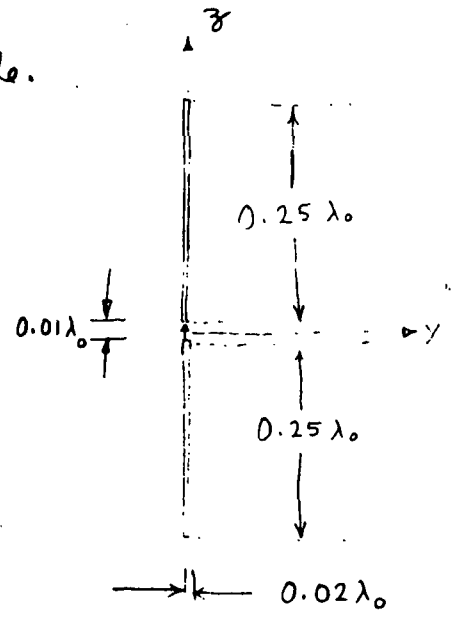

Fig. 1.5(a)

ORIGINAL PAGE IS
OF POOR QUALITY

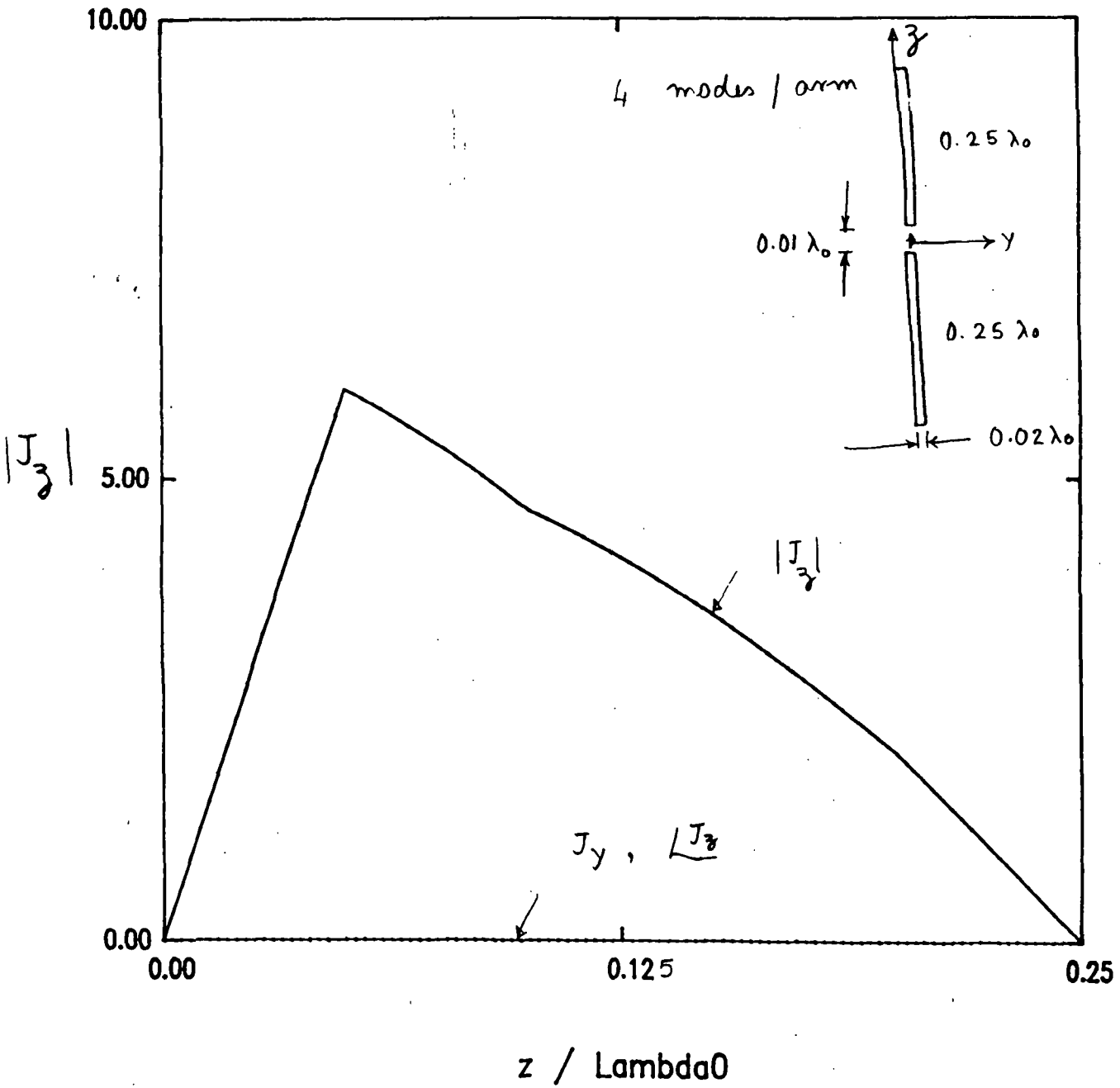
10.00
5.00
0.00
0.00
0.125
0.25
z / Lambda0
|J_z|
4 modes / arm
z
y
0.25 λ0
0.01 λ0
0.25 λ0
0.02 λ0
|J_z|
J_y , ∠J_z

Fig. 1.5(b)

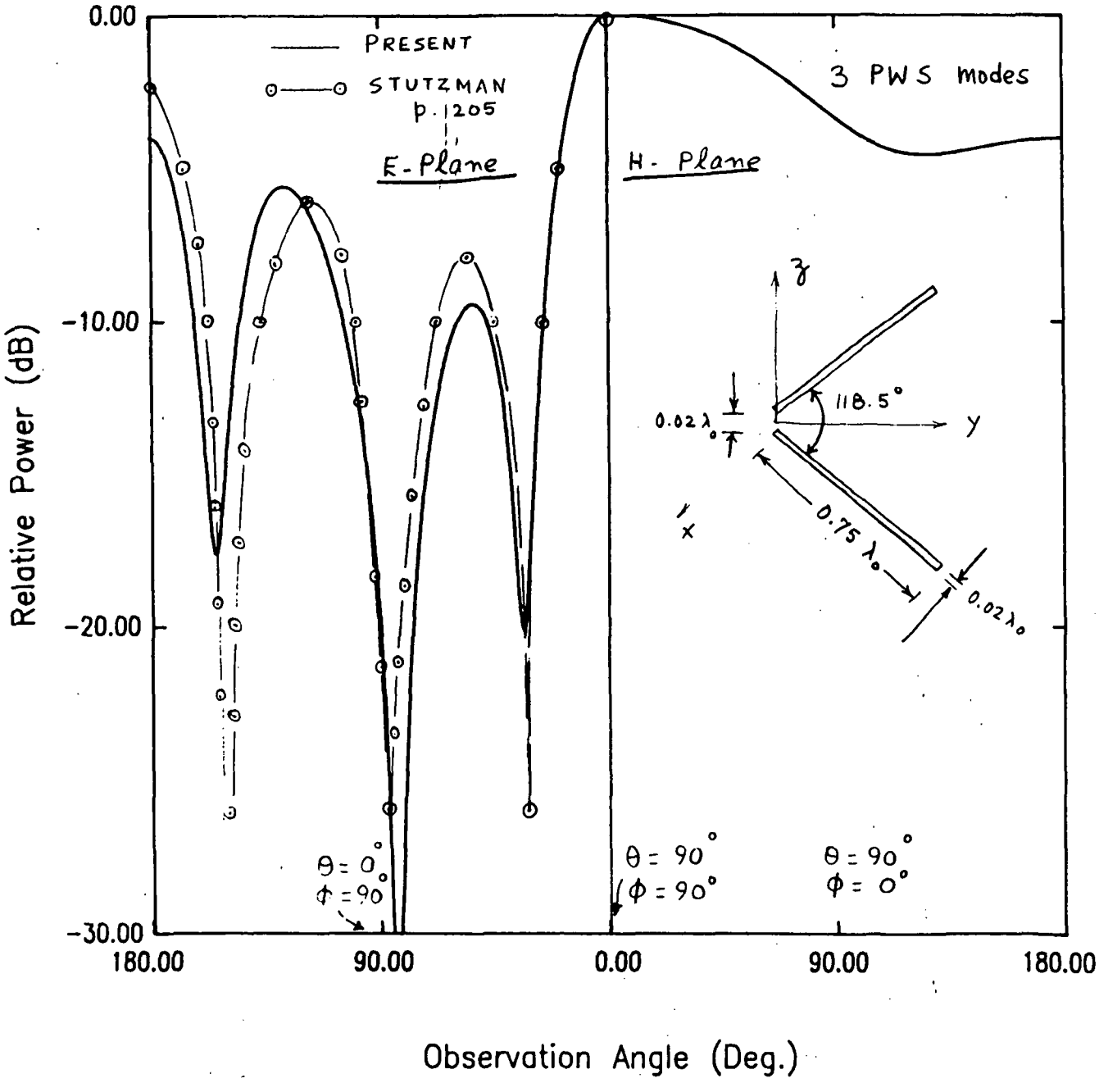
0.00
-10.00
-20.00
-30.00
Relative Power (dB)
PRESENT
STUTZMAN
p. 1205
E-Plane
H-Plane
3 PWS modes
z
y
x
118.5°
0.02 λ₀
0.75 λ₀
0.02 λ₀
θ = 0°
φ = 90°
θ = 90°
φ = 90°
θ = 90°
φ = 0°
180.00
90.00
0.00
90.00
180.00
Observation Angle (Deg.)

Fig. 1.6

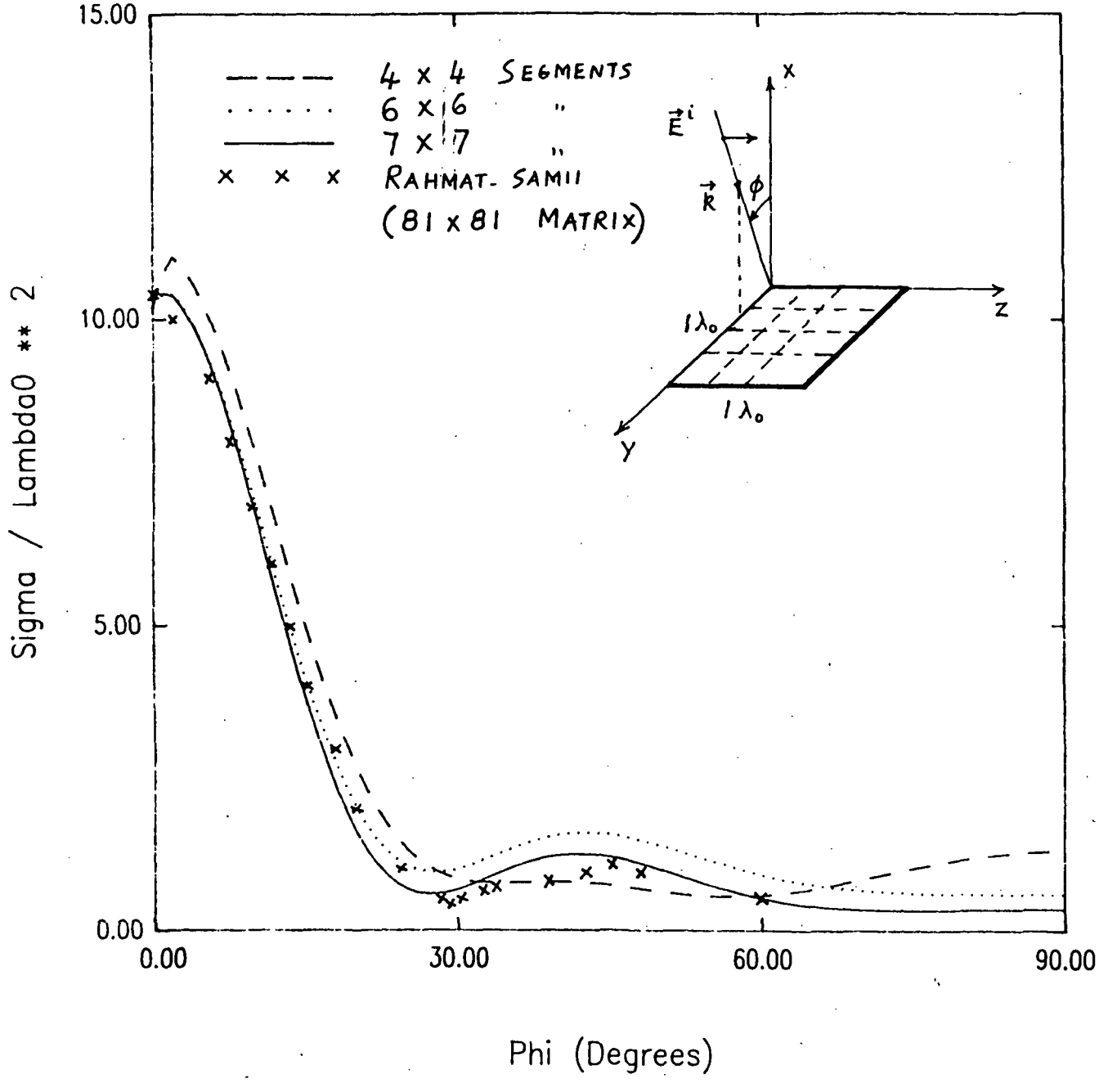
15.00
10.00
5.00
0.00
0.00
30.00
60.00
90.00
Sigma / Lambda0 ** 2
Phi (Degrees)
4 x 4 SEGMENTS
6 x 6 "
7 x 7 "
RAHMAT- SAMII
(81 x 81 MATRIX)
x
z
y
$\vec{E}^i$
$\vec{k}$
ϕ
$1\lambda_0$
$1\lambda_0$

Fig. 1.7

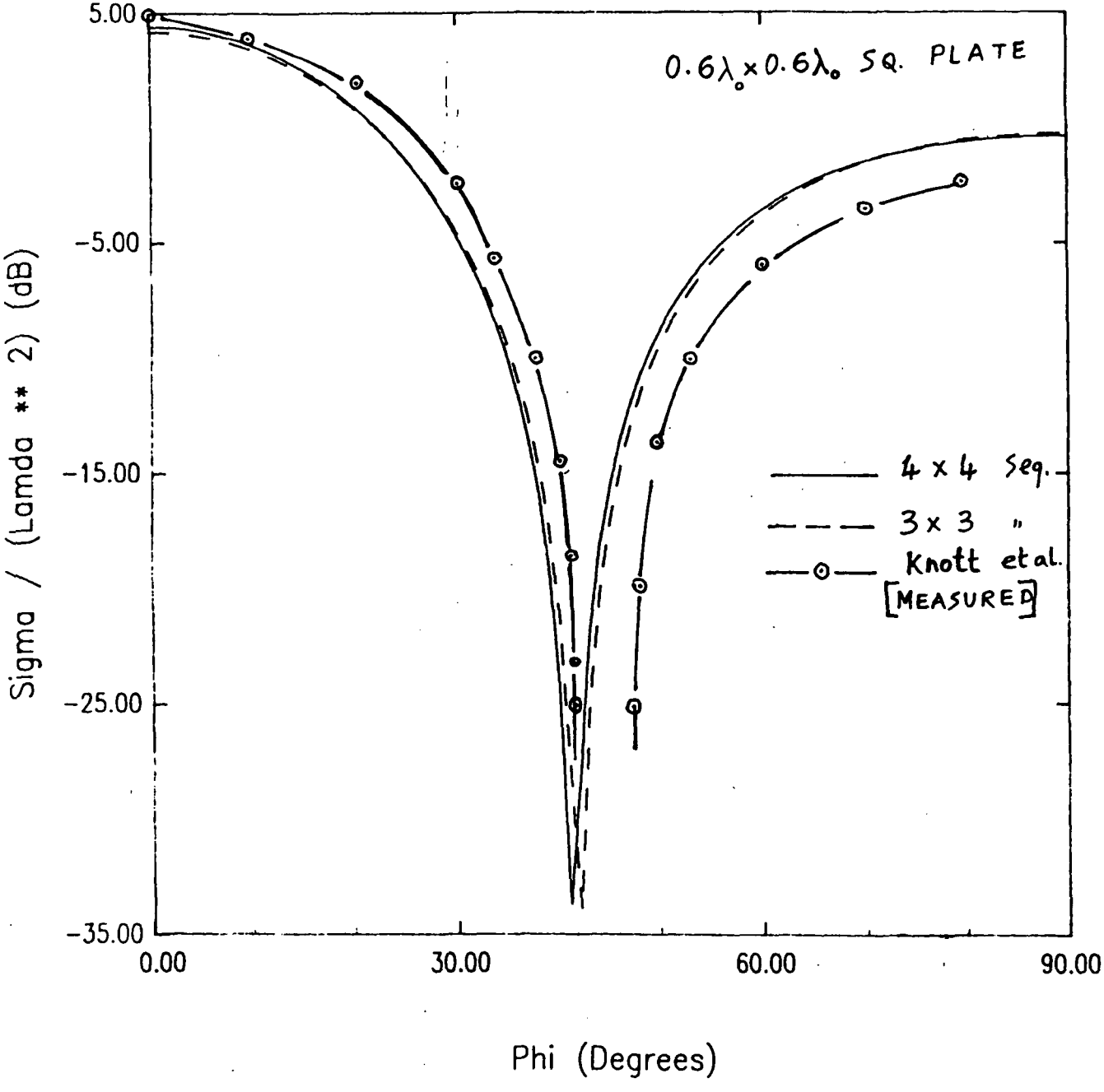
5.00
-5.00
-15.00
-25.00
-35.00
0.00
30.00
60.00
90.00
Sigma / (Lamda ** 2) (dB)
Phi (Degrees)
0.6λ₀ × 0.6λ₀ SQ. PLATE
4 x 4 Seq.
3 x 3 "
Knott et al.
[MEASURED]

Fig. 1.8

LTSA L_{12}

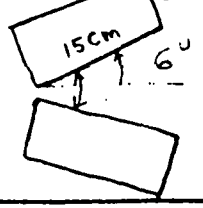

LTSA L_{12} $f = 6.0$ GHz

E–Plane

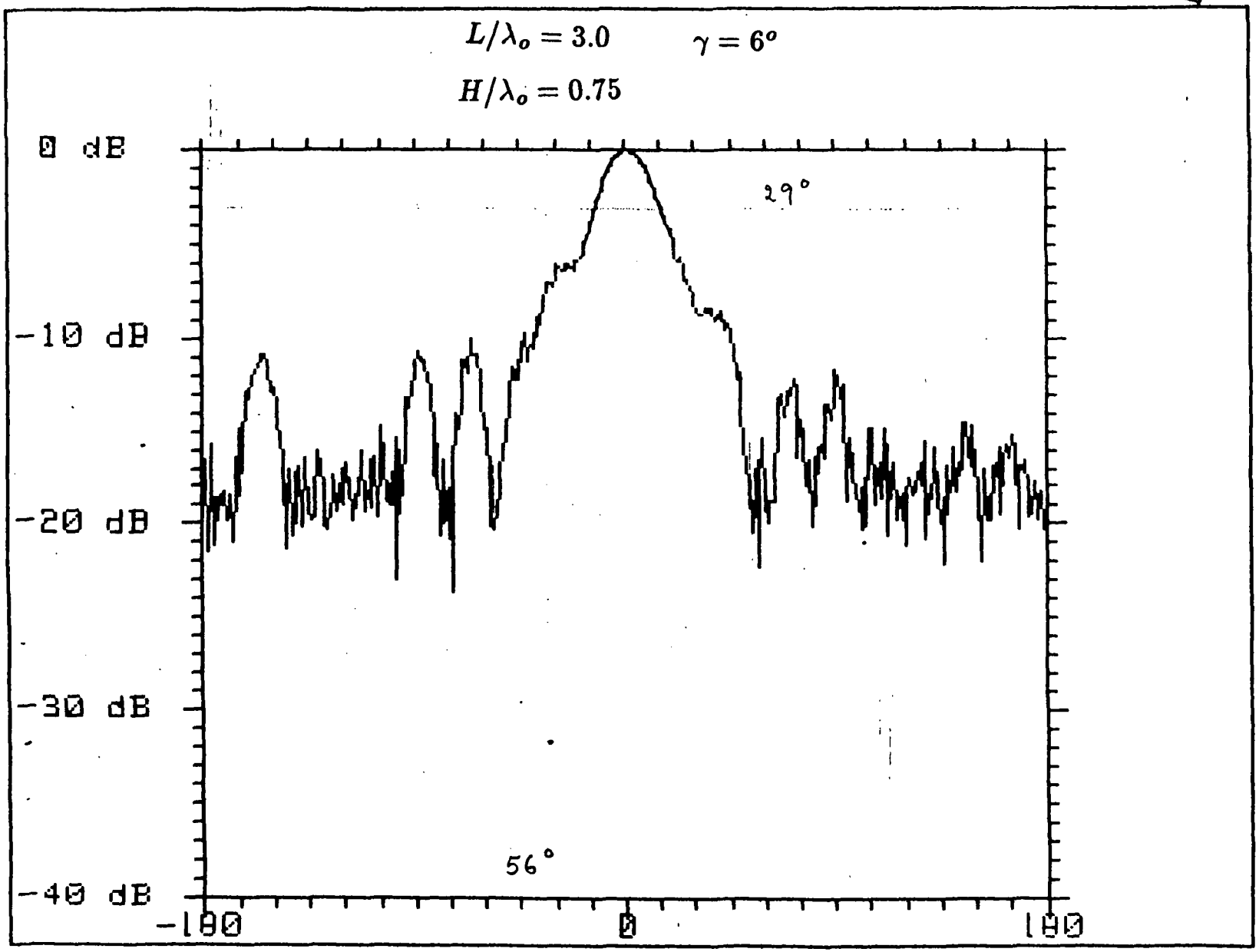

Fig. 1.9(a)

LTSA L_{12}, 6.0 GHz, H–Plane

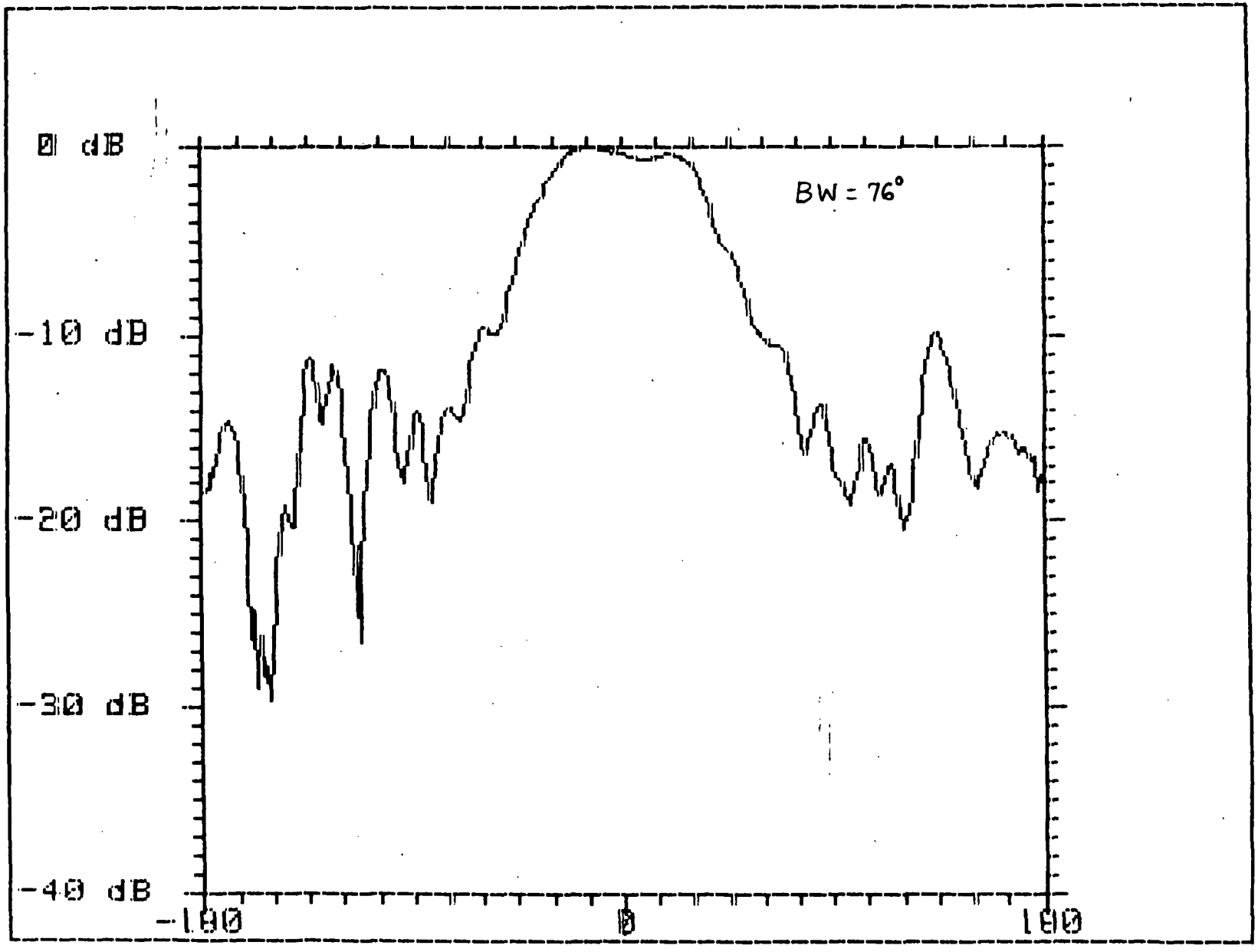

Fig. 1.9(b)

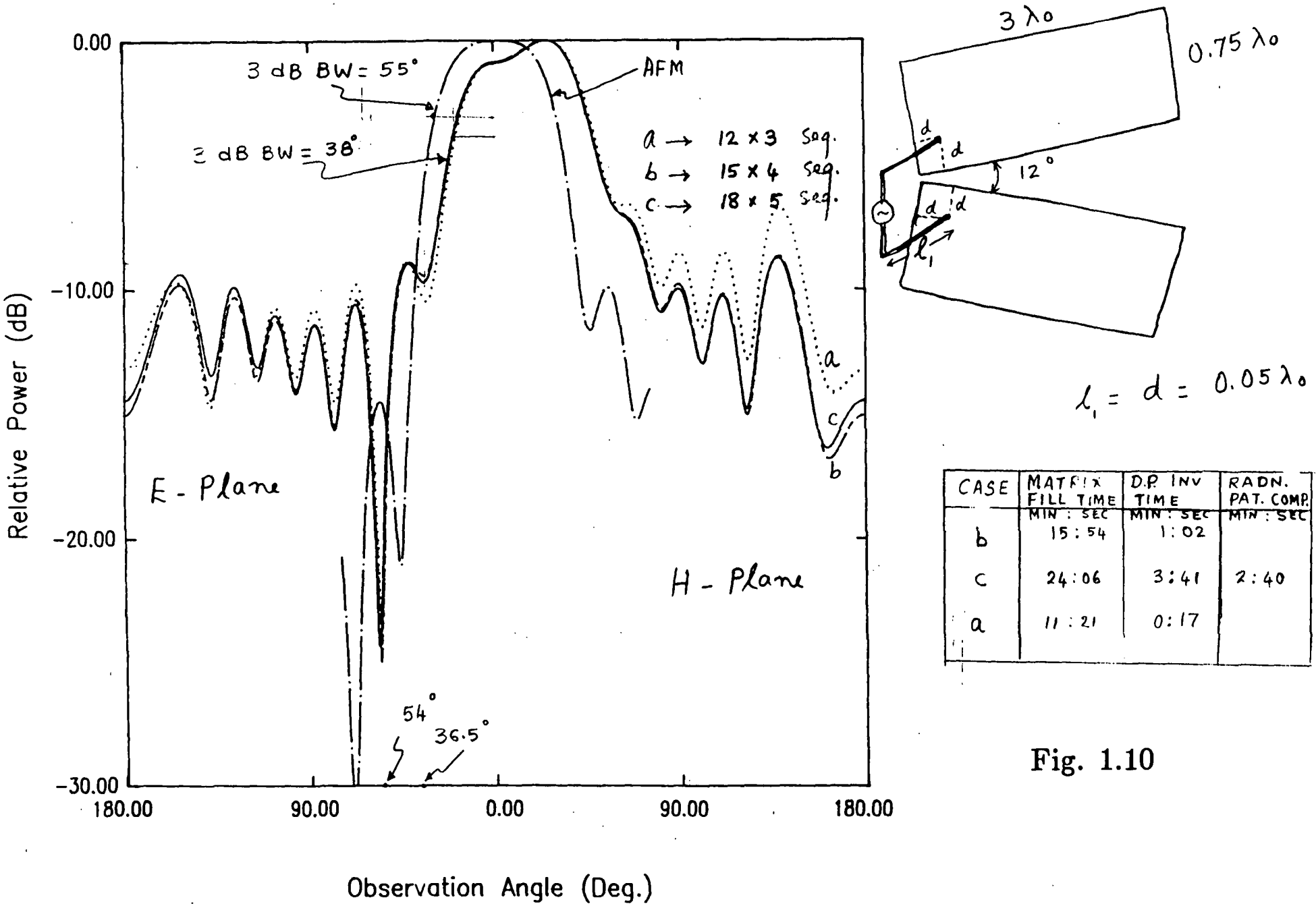

CASE	MATRIX FILL TIME MIN : SEC	D.P. INV TIME MIN : SEC	RADN. PAT. COMP. MIN : SEC
b	15 : 54	1 : 02	
c	24 : 06	3 : 41	2 : 40
a	11 : 21	0 : 17	

Fig. 1.10

ORIGINAL PAGE IS
OF POOR QUALITY

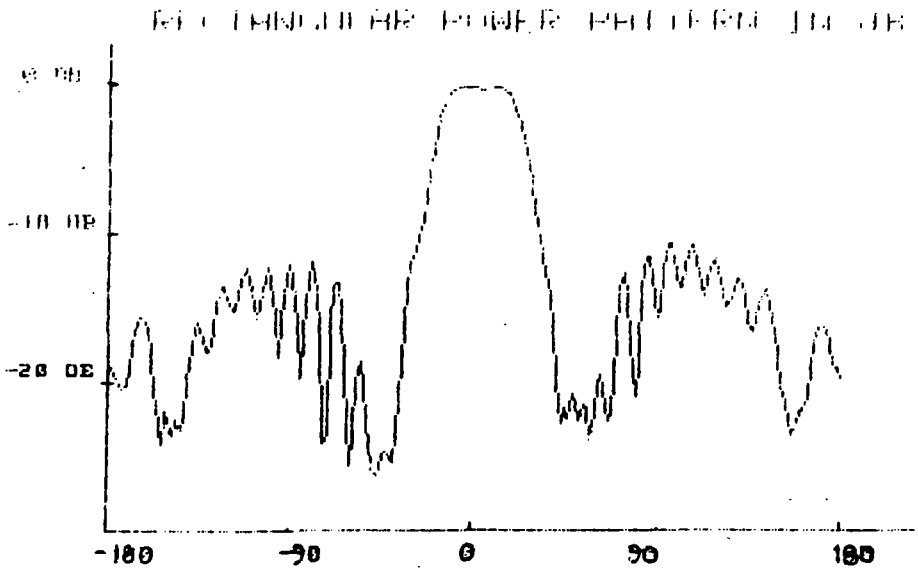

$BW = 45^o$

E–Plane

$L/\lambda_o = 4.8$

$\gamma = 5.9^o$

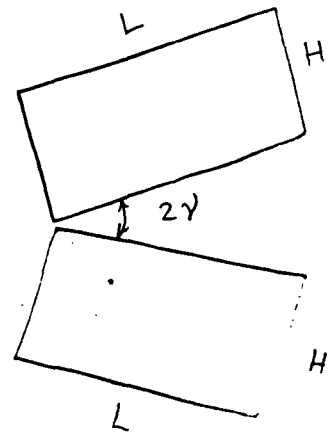

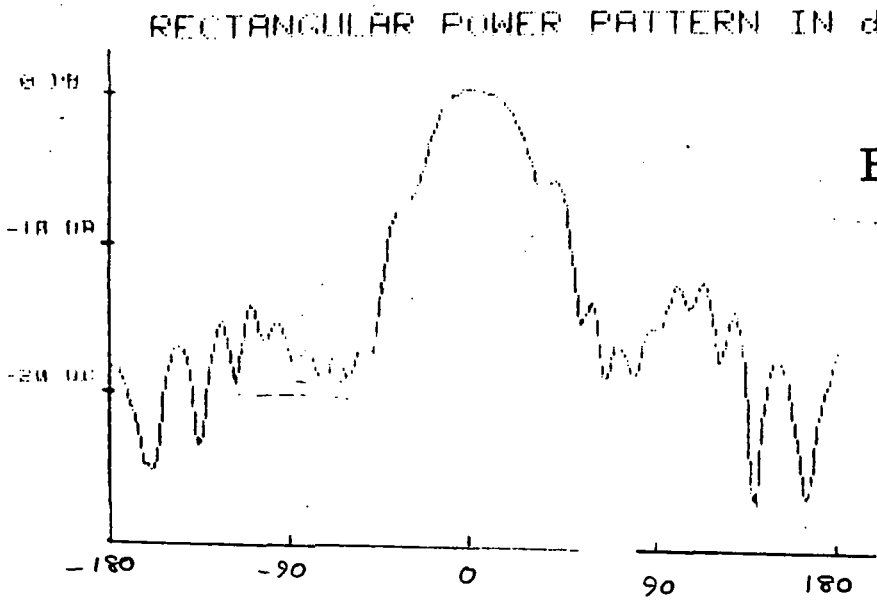

$BW = 45^o$

H–Plane

$H/\lambda_o = 2.1$

Fig. 1.11(a)

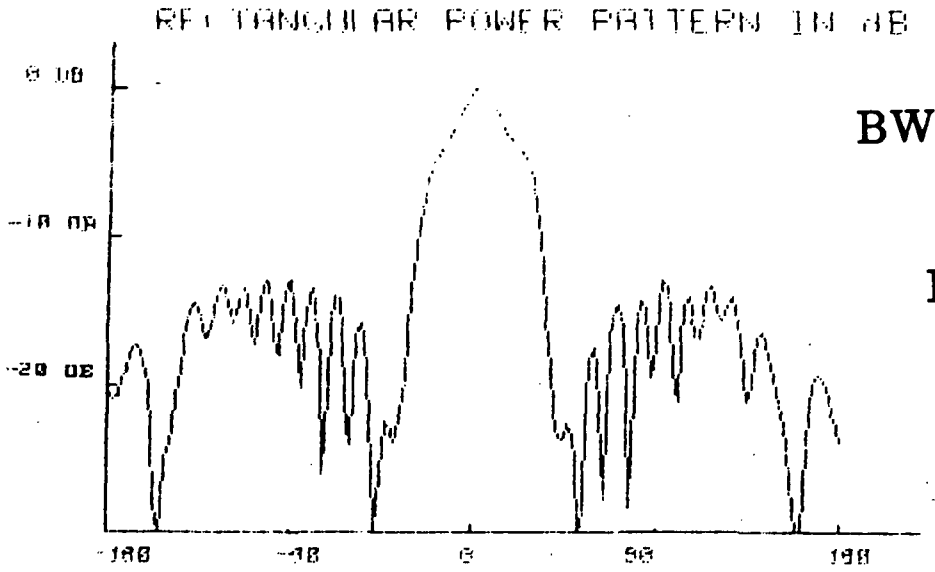

BW = 29°

E–Plane

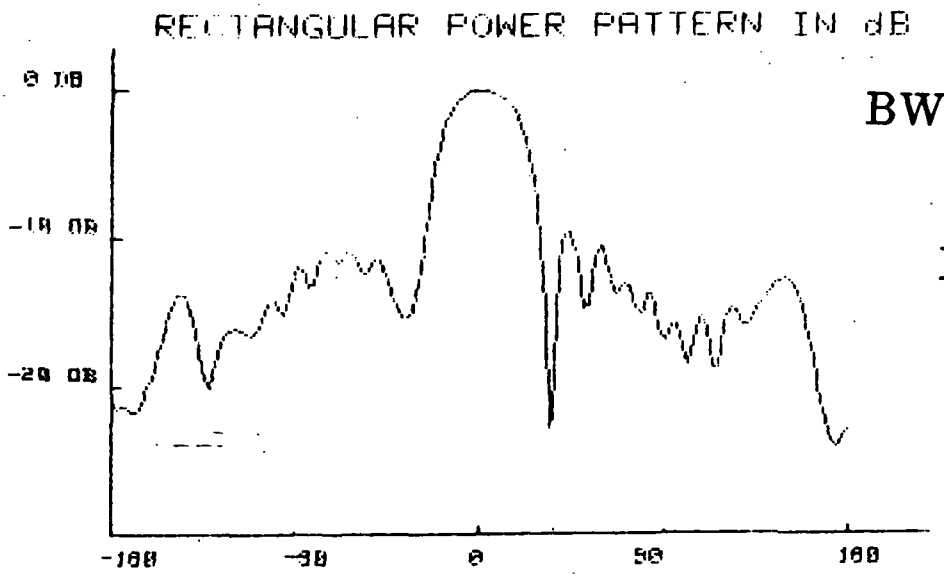

BW = 44°

H–Plane

Fig. 1.11(b)

$H/\lambda_o = 1.33$

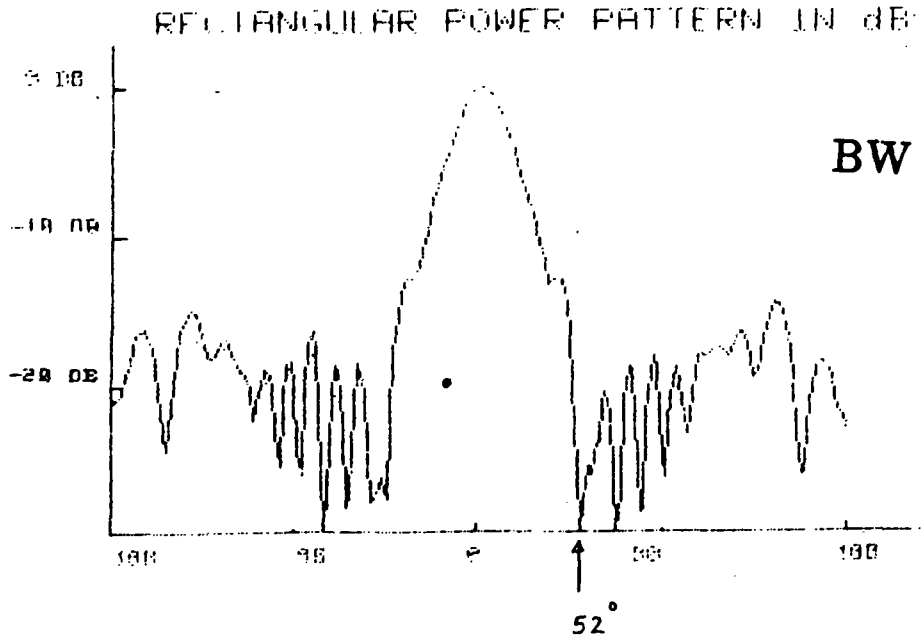

BW = 29°

E–Plane

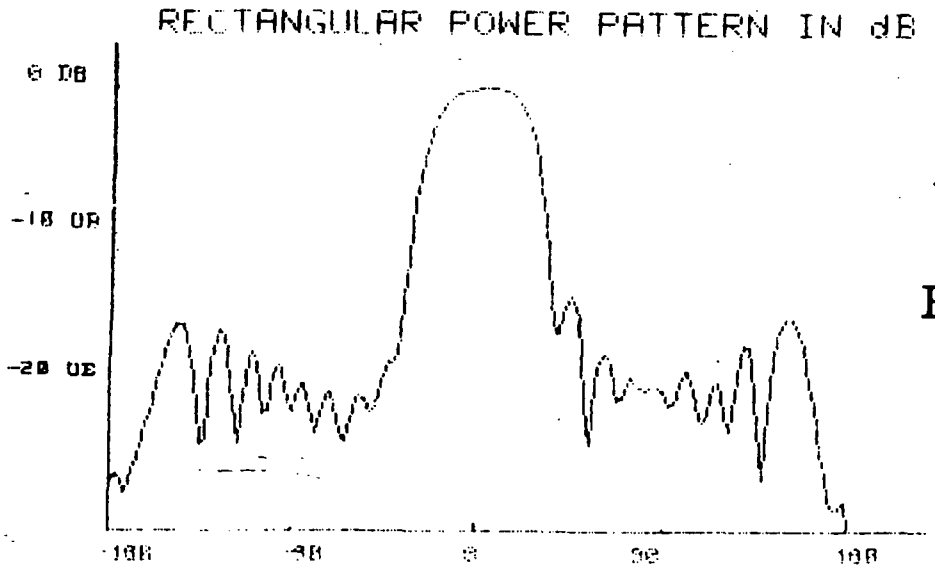

BW = 52°

H–Plane

Fig. 1.11(c)

$H/\lambda_o = 1.0$

ORIGINAL PAGE IS
OF POOR QUALITY

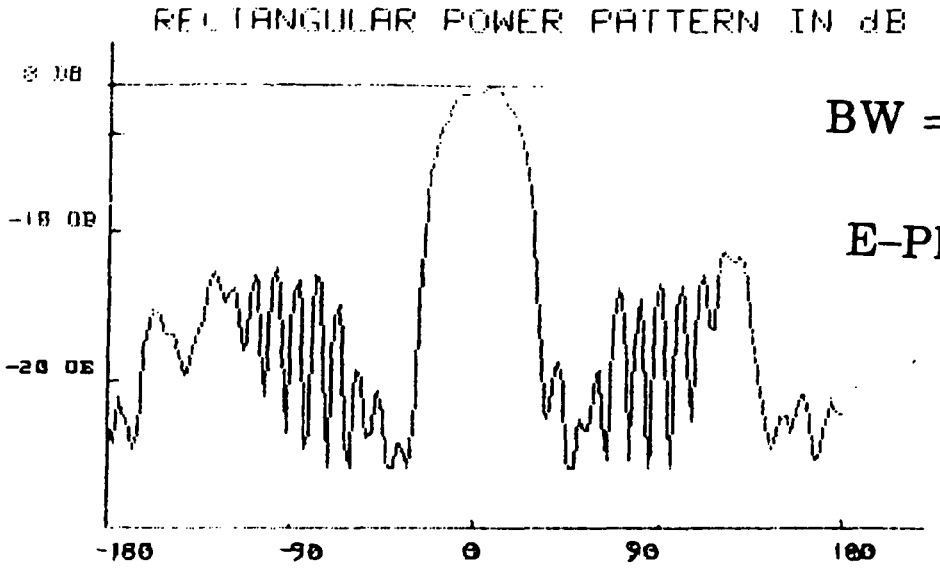

$BW = 40^o$

E–Plane

$L/\lambda_o = 5.2$

$\gamma = 7^o$

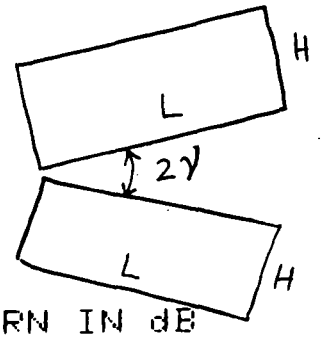

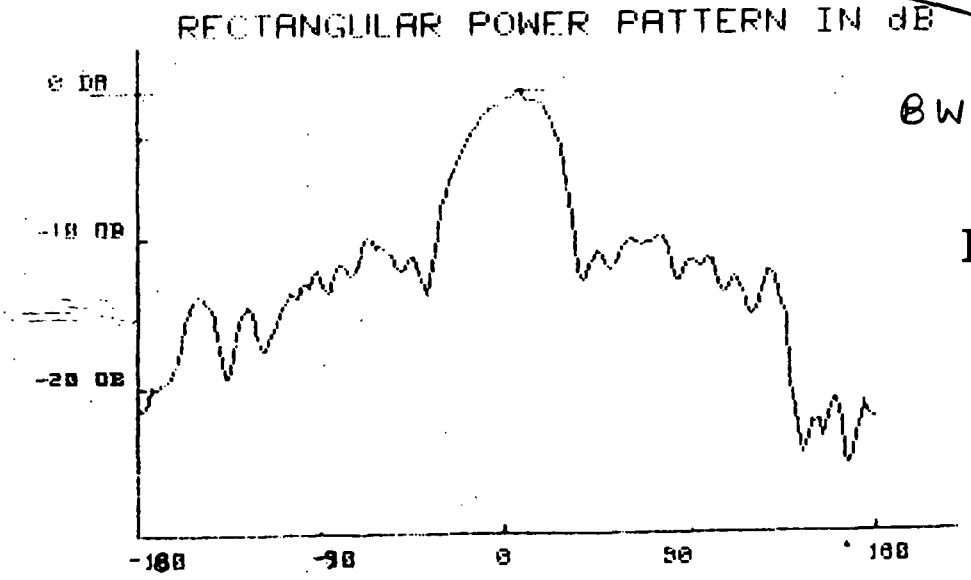

$BW = 44^\circ$

H–Plane

$H/\lambda_o = 2.46$

Fig. 1.12(a)

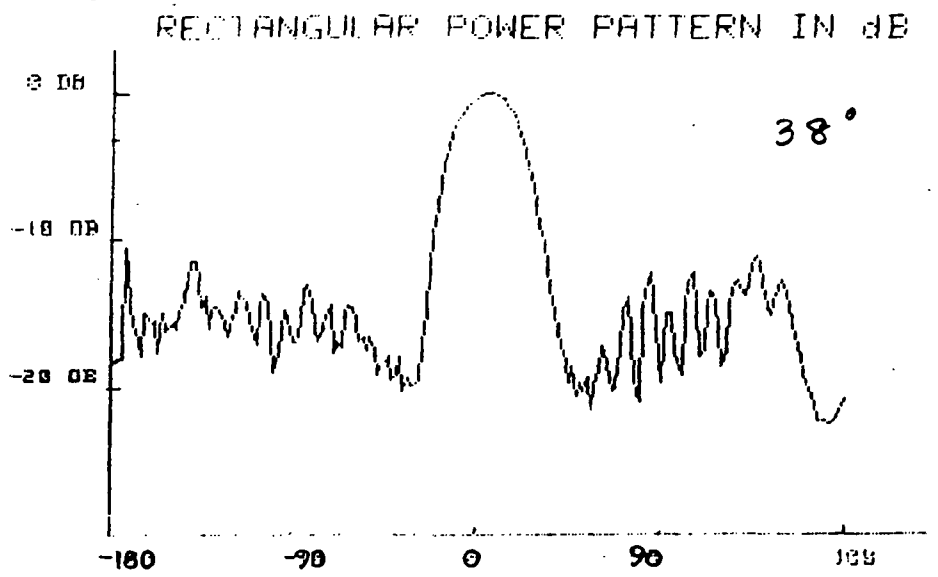

E–Plane

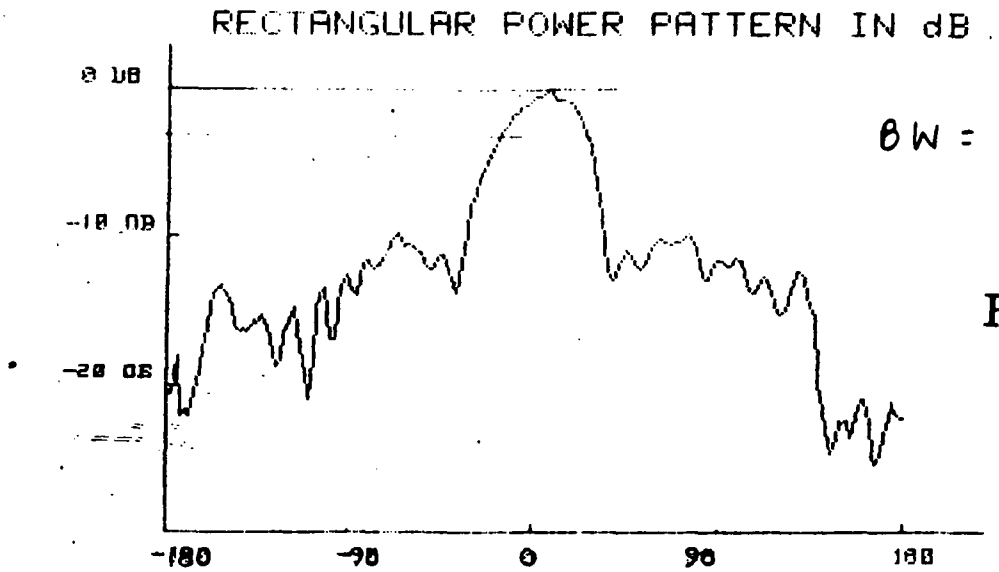

H–Plane

$H/\lambda_o = 1.5$

Fig. 1.12(b)

E–Plane

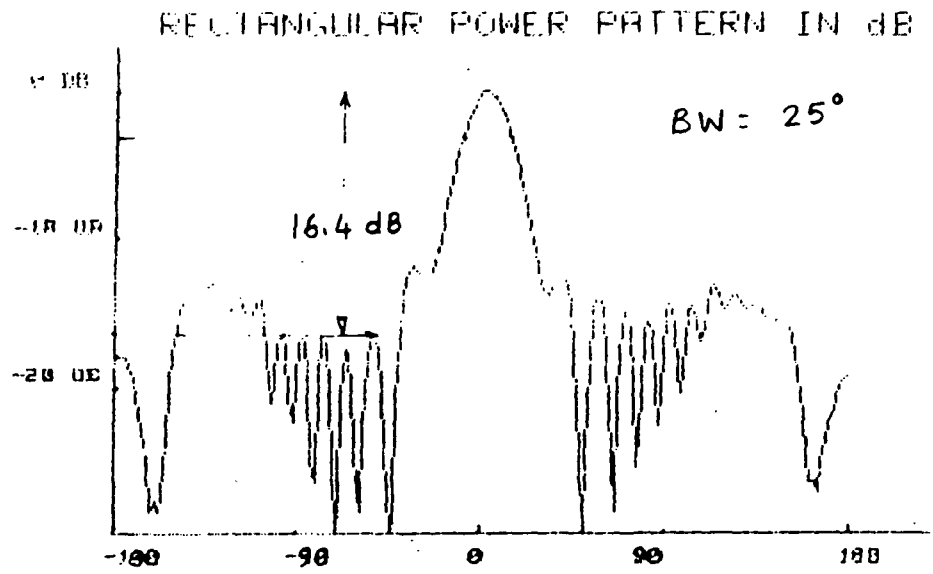

H–Plane

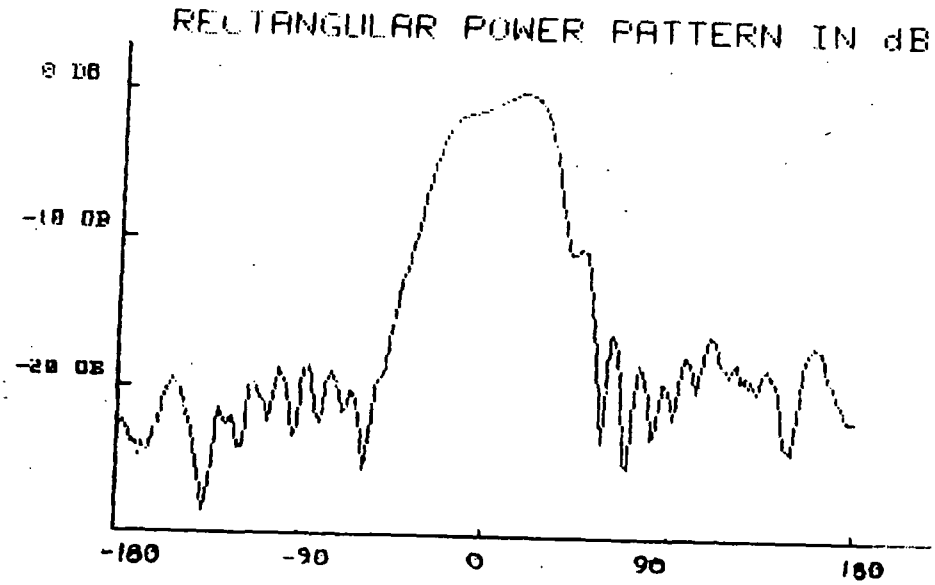

$H/\lambda_o = 0.9$

Fig. 1.12(c)

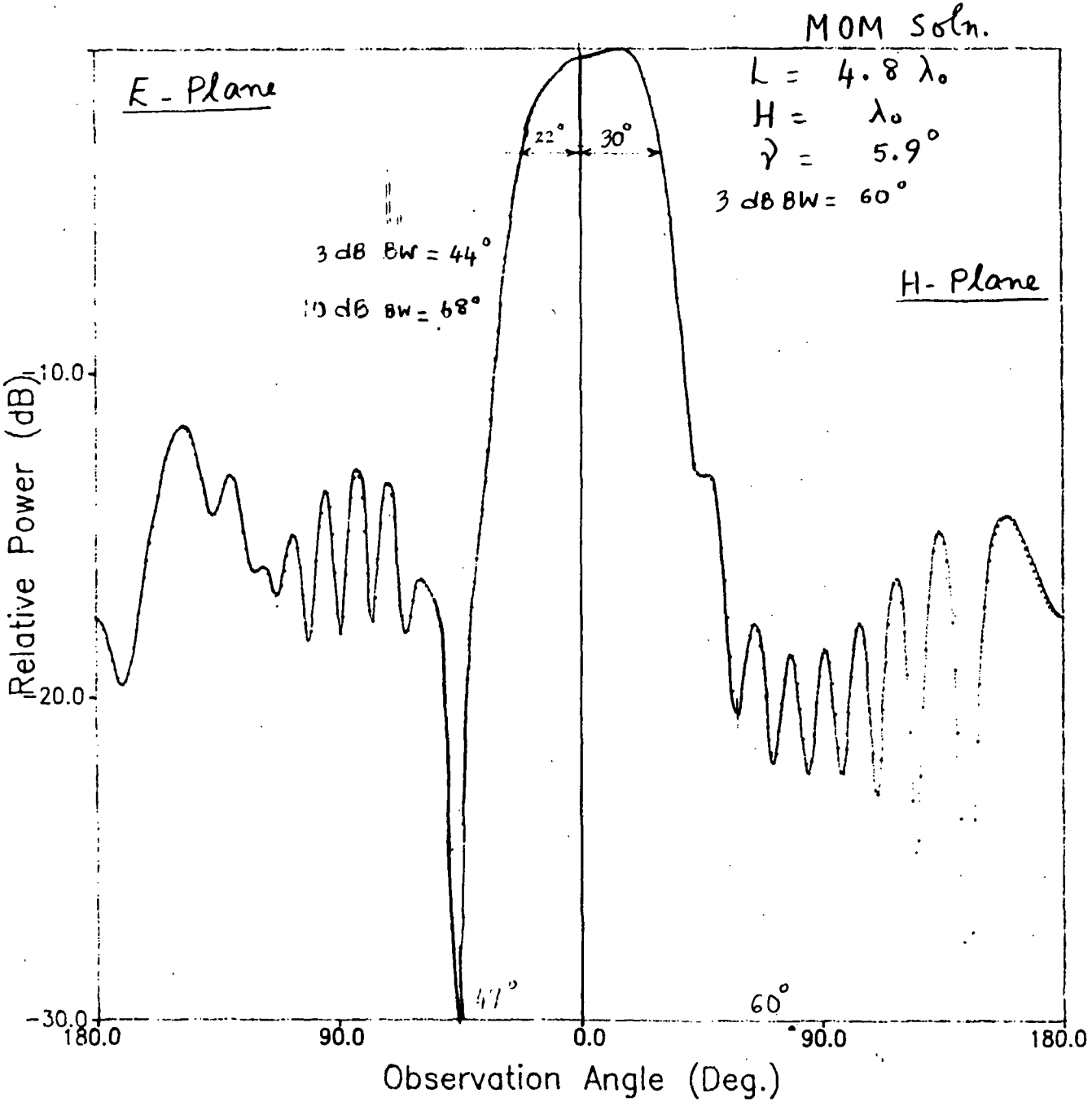
MOM Soln.
E - Plane
L = 4.8 λ₀
H = λ₀
γ = 5.9°
3 dB BW = 60°
22°
30°
3 dB BW = 44°
10 dB BW = 68°
H - Plane
10.0
20.0
-30.0
Relative Power (dB)
47°
60°
180.0
90.0
0.0
90.0
180.0
Observation Angle (Deg.)

Fig. 1.13(a)

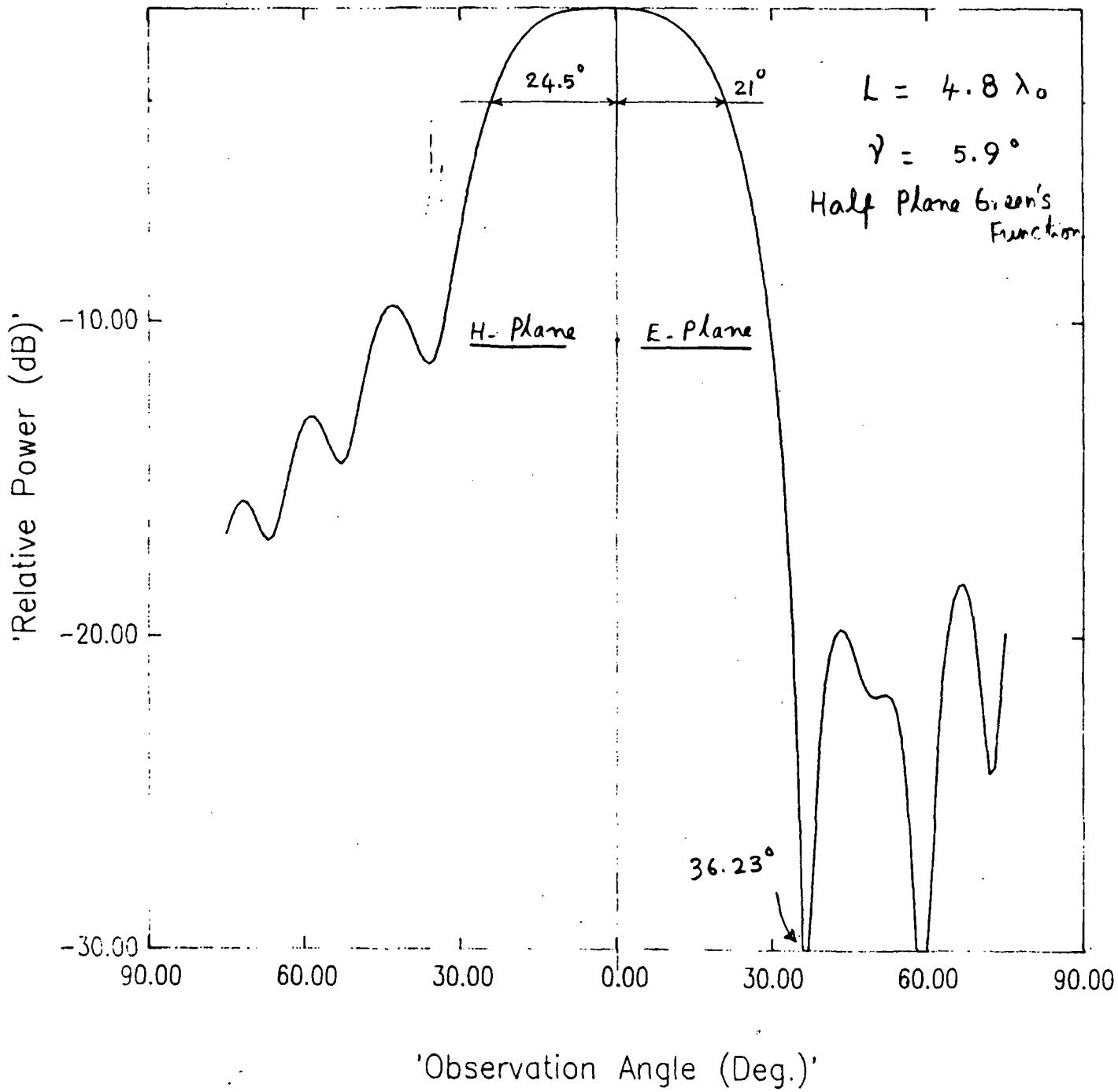
24.5°
21°
L = 4.8 λ₀
γ = 5.9°
Half Plane Green's Function
H- Plane
E- Plane
36.23°
'Relative Power (dB)'
-10.00
-20.00
-30.00
90.00
60.00
30.00
0.00
30.00
60.00
90.00
'Observation Angle (Deg.)'

Fig. 1.13(b)

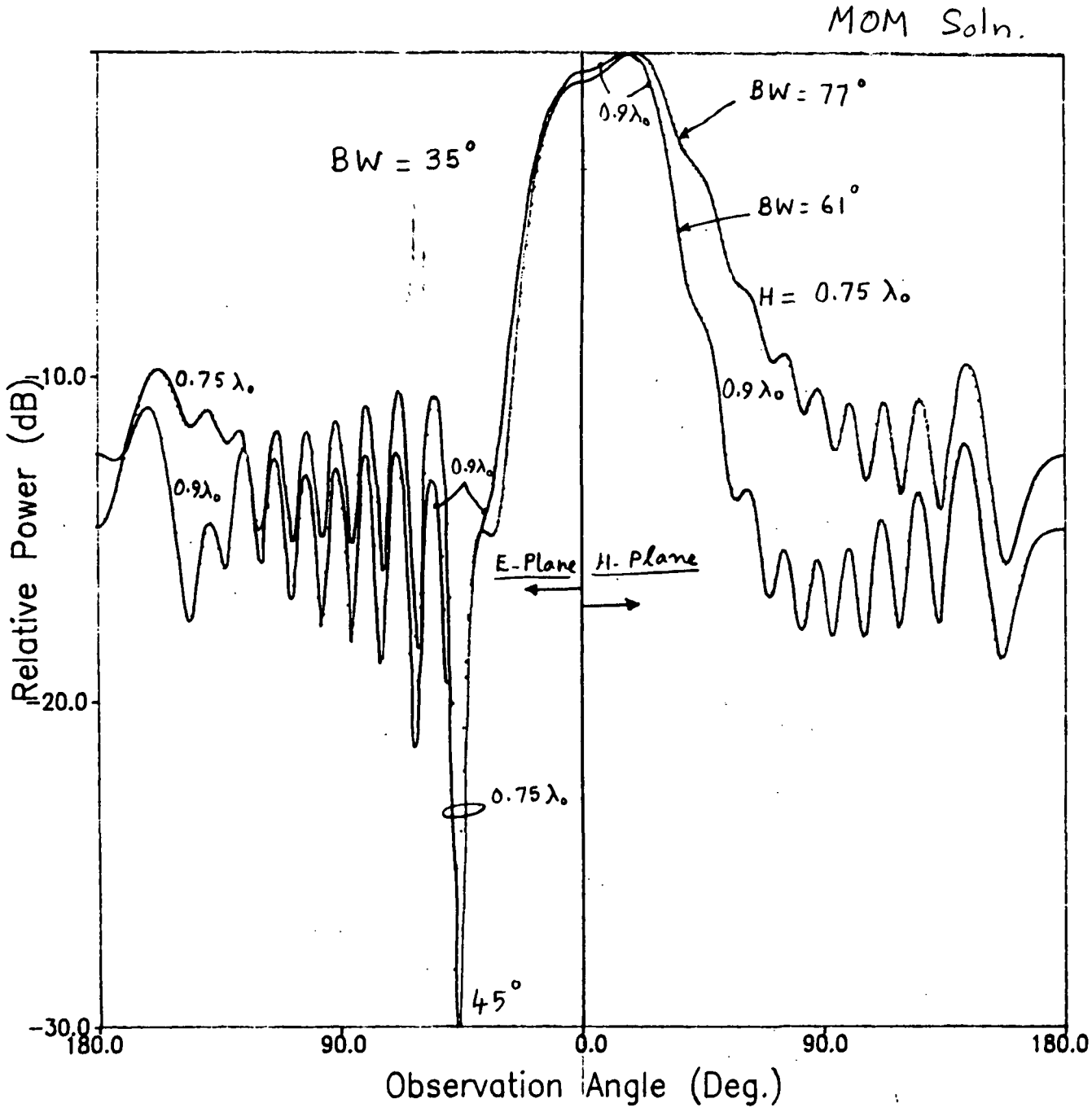

$L = 5.16\ \lambda_o$

$\gamma = 7^o$

Fig. 1.14

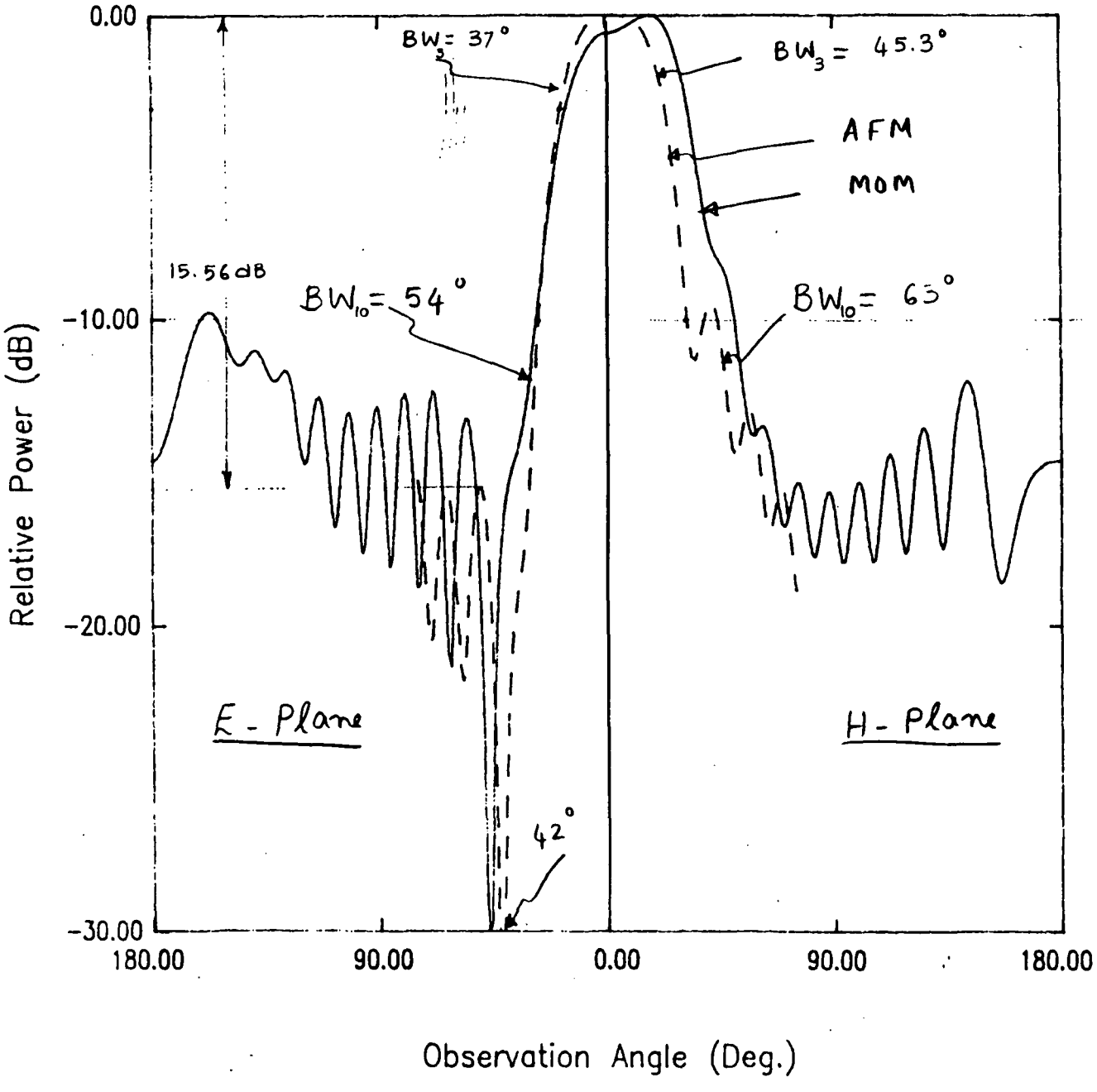
0.00
-10.00
-20.00
-30.00
180.00
90.00
0.00
90.00
180.00
Relative Power (dB)
Observation Angle (Deg.)
BW3 = 37°
BW3 = 45.3°
AFM
MOM
15.56dB
BW10 = 54°
BW10 = 63°
E - Plane
H - Plane
42°

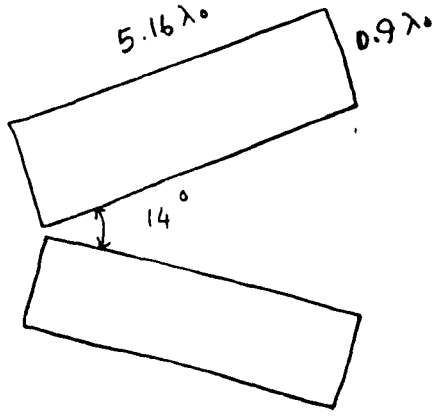
5.16λ0
0.9λ0
14°

Fig. 1.15

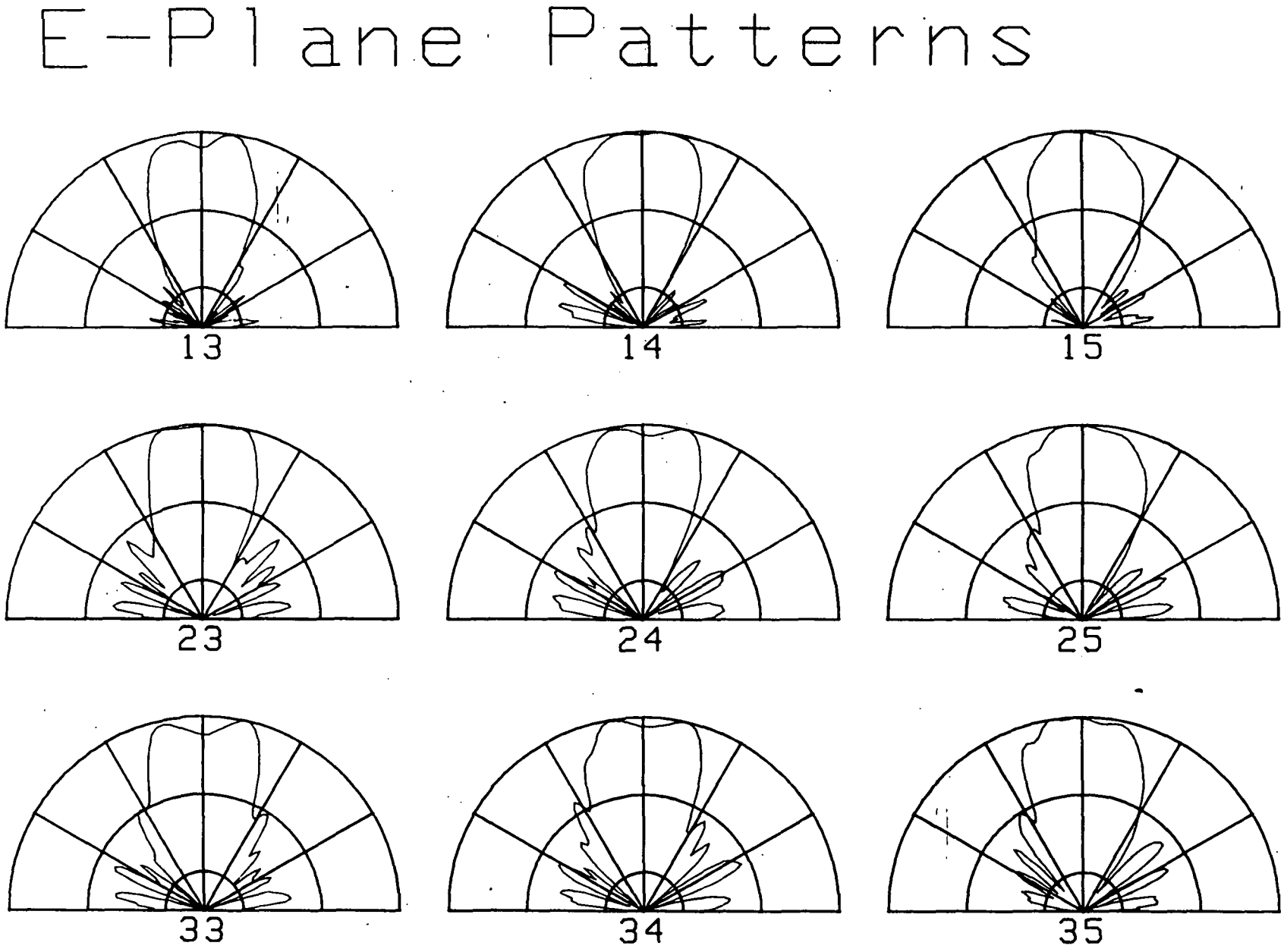

Figure 2.1.a

H-Plane Patterns

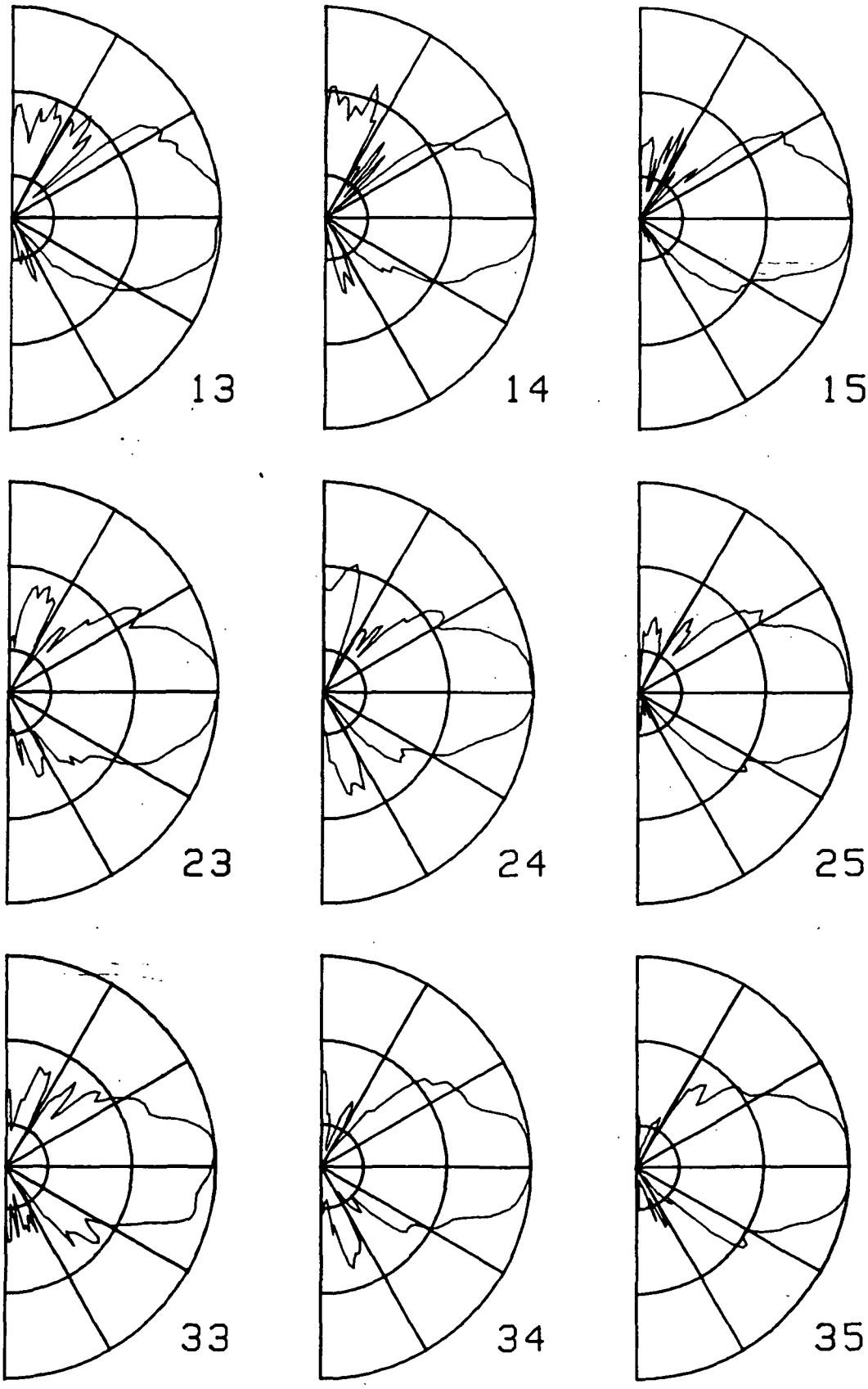

Figure 2.1.b

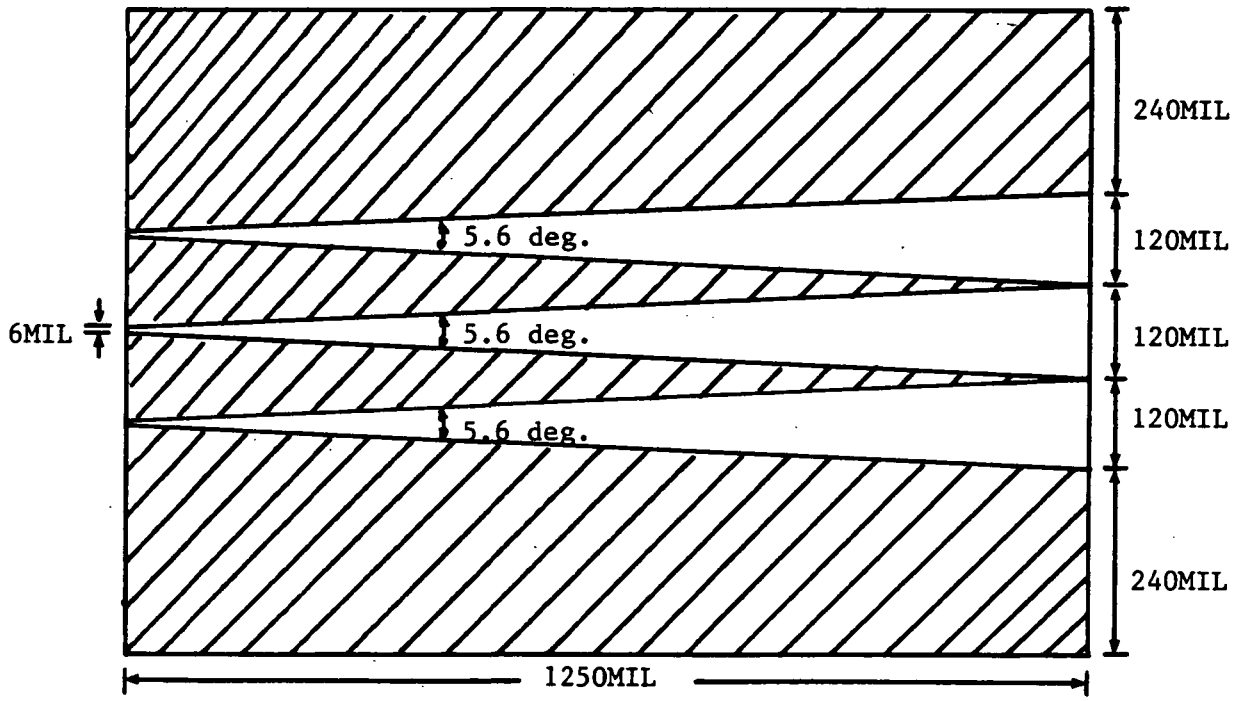
240MIL
5.6 deg.
120MIL
6MIL
5.6 deg.
120MIL
5.6 deg.
120MIL
240MIL
1250MIL

Figure 2.2

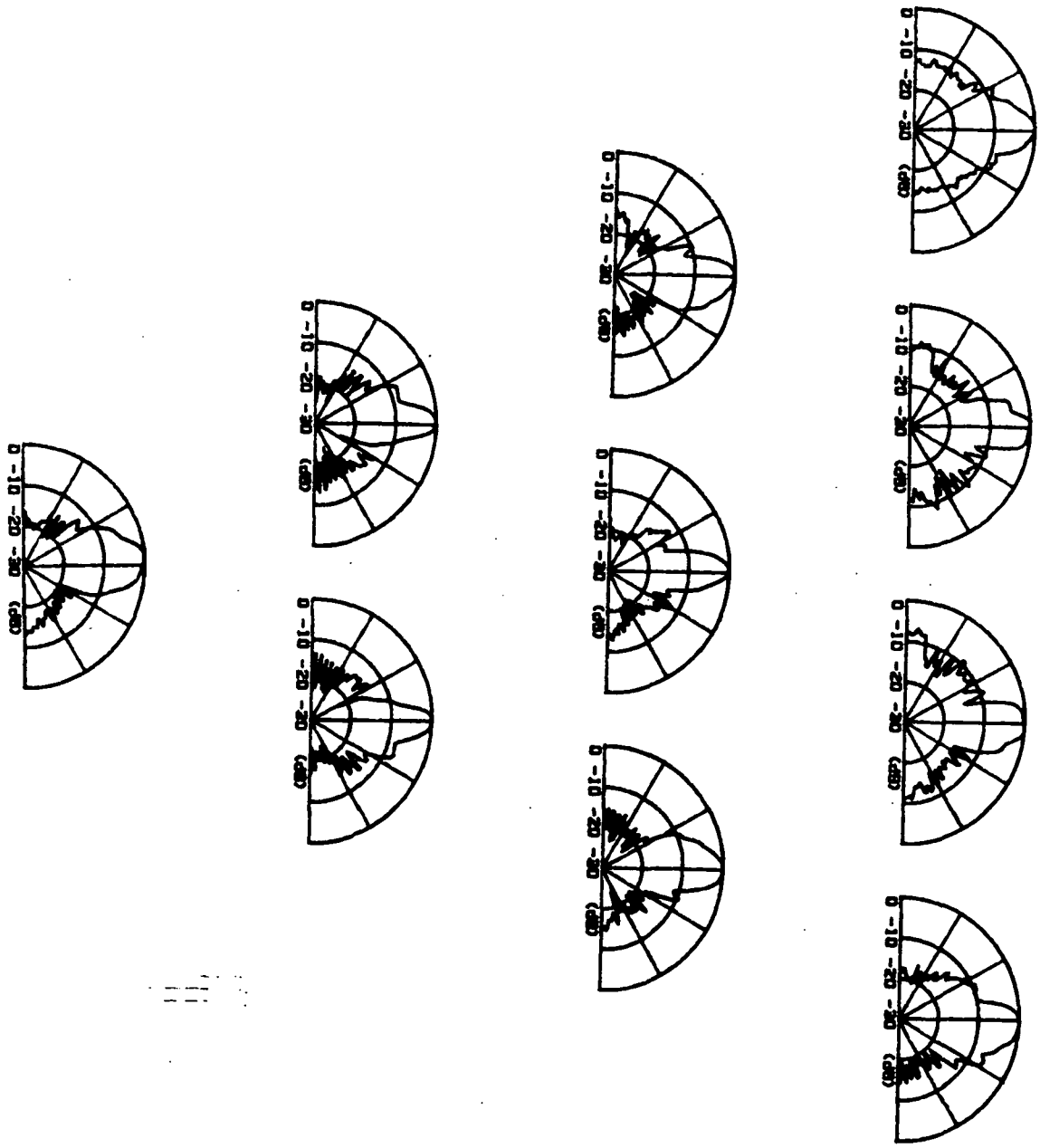

(a)

Figure 2.3.

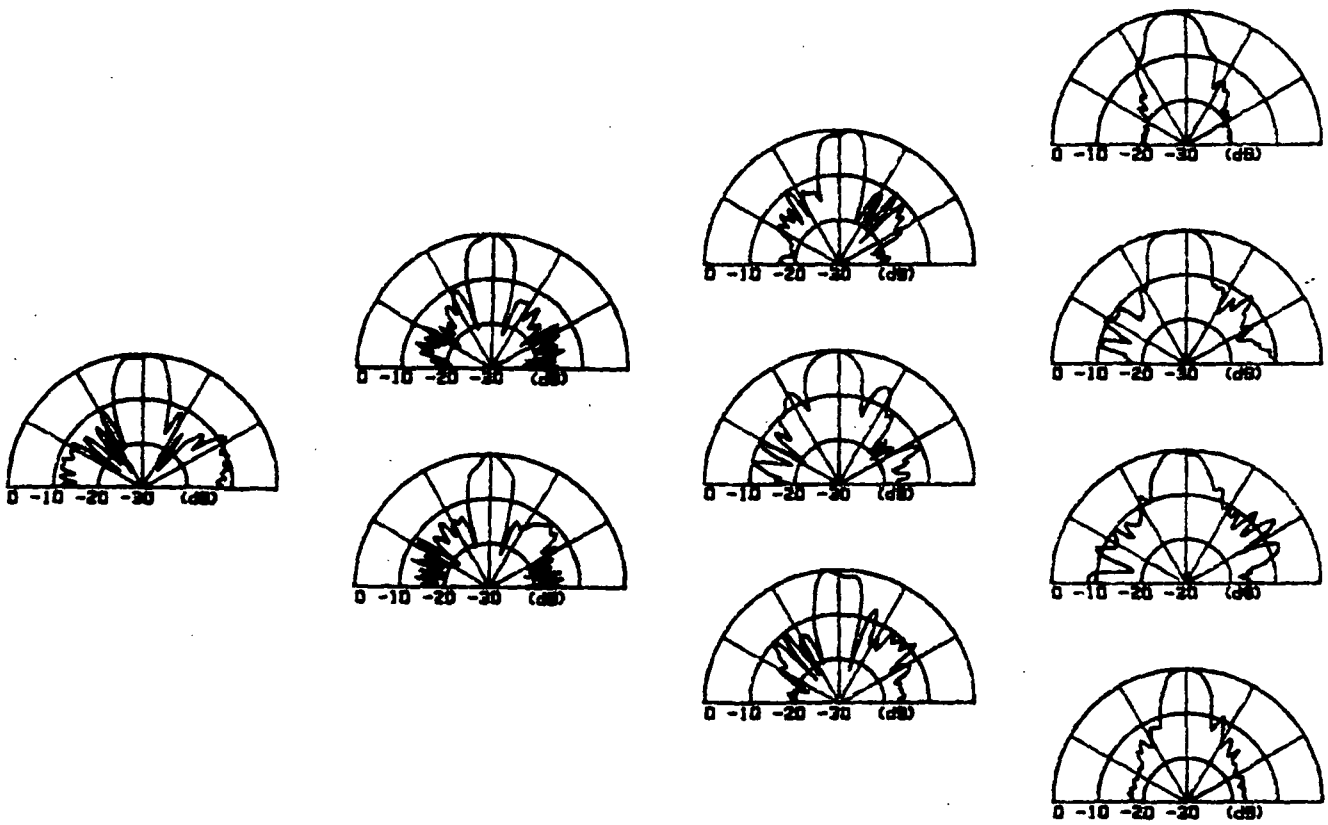

(b)

Figure 2.3.

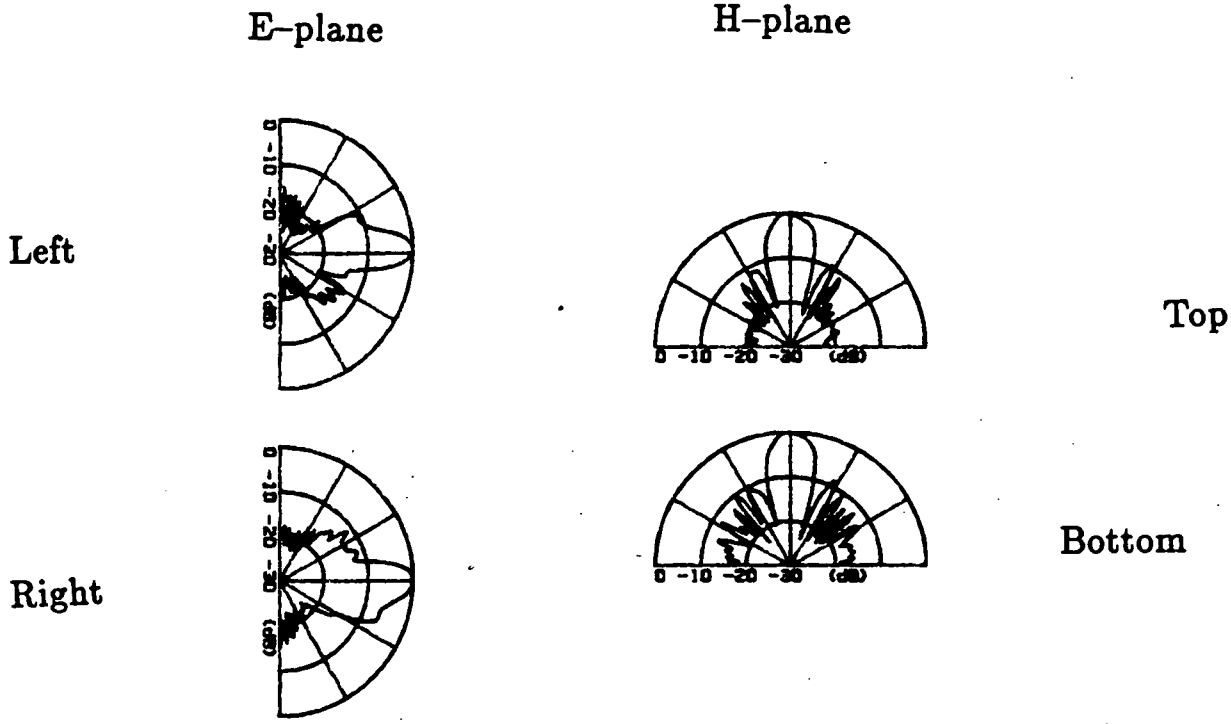

Figure 2.4.

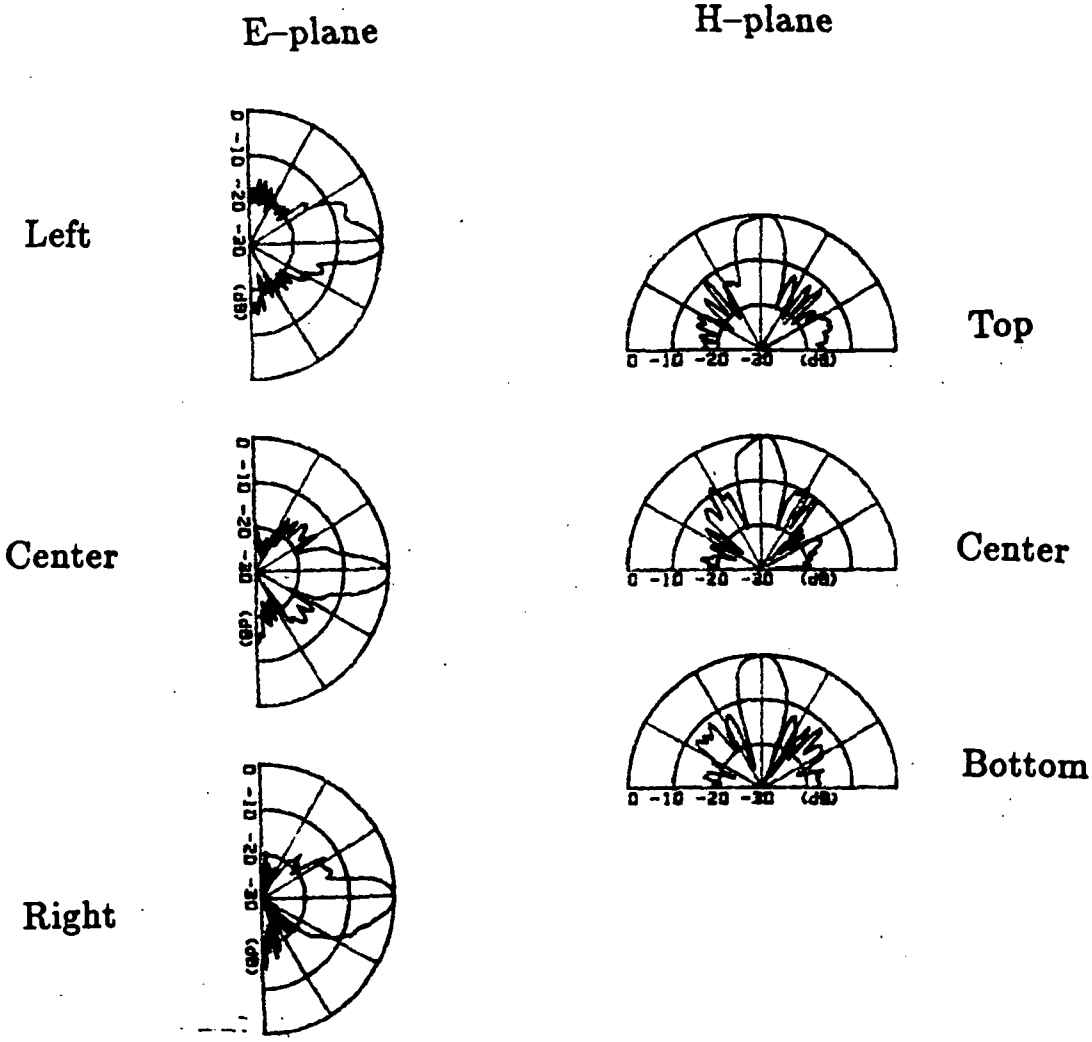
E–plane
H–plane
Left
Center
Right
Top
Center
Bottom
0 -10 -20 -30 (dB)

Figure 2.5.

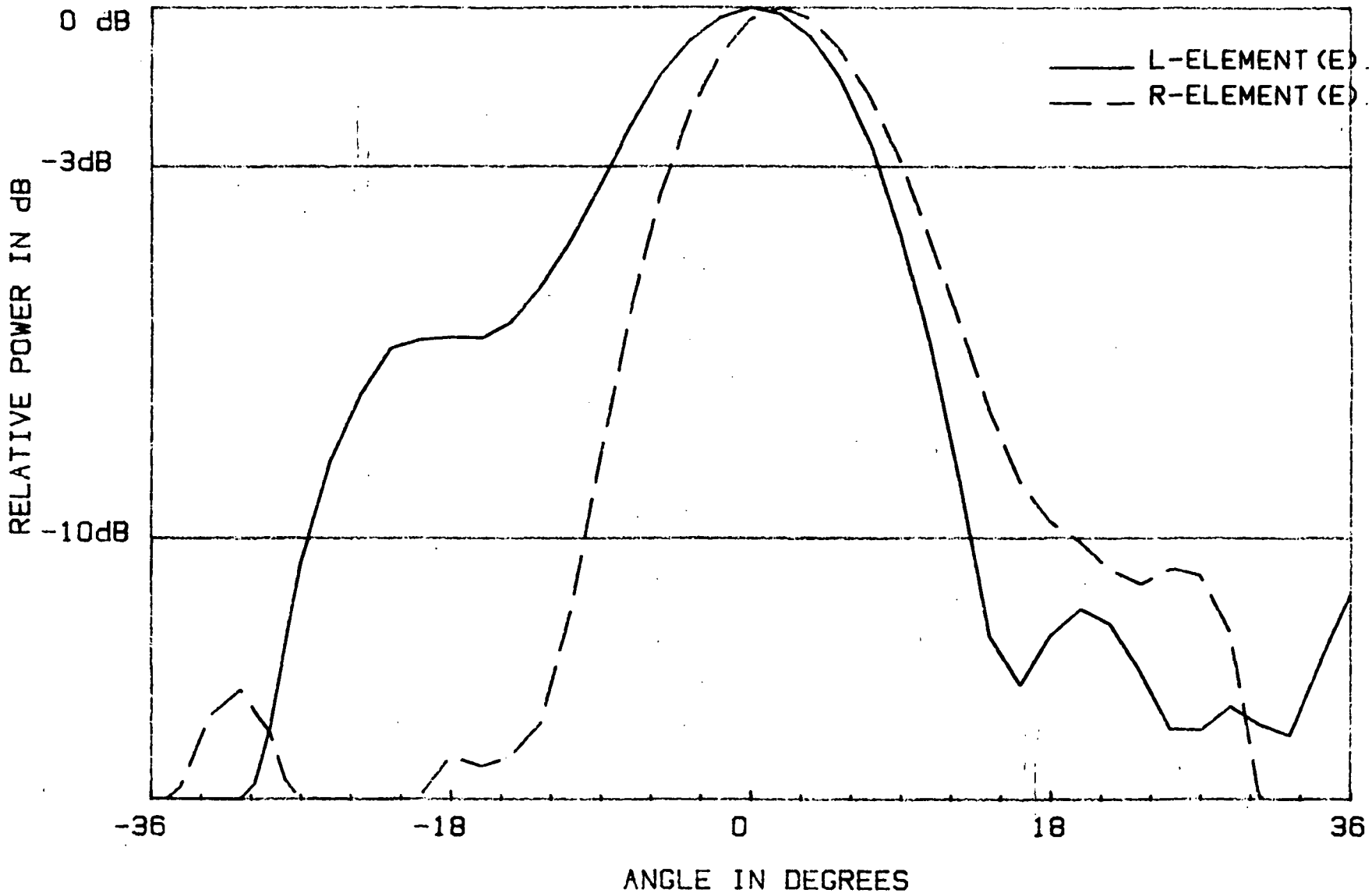
0 dB
-3dB
-10dB
RELATIVE POWER IN dB
L-ELEMENT (E)
R-ELEMENT (E)
-36
-18
0
18
36
ANGLE IN DEGREES

(a)

Figure 2.6.

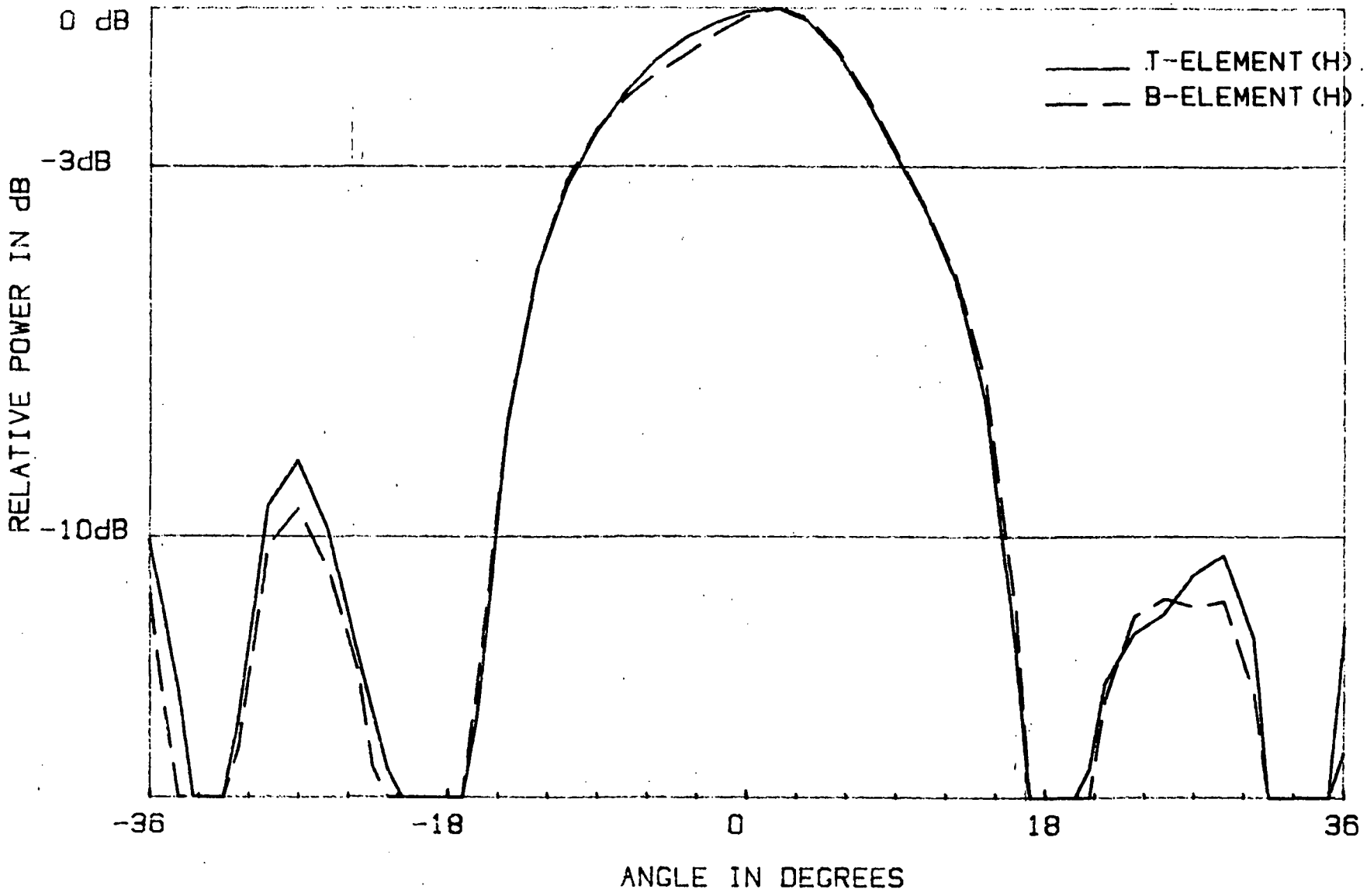
0 dB
-3dB
-10dB
RELATIVE POWER IN dB
T-ELEMENT (H)
B-ELEMENT (H)
-36
-18
0
18
36
ANGLE IN DEGREES

(b)

Figure 2.6.

E–PLANE

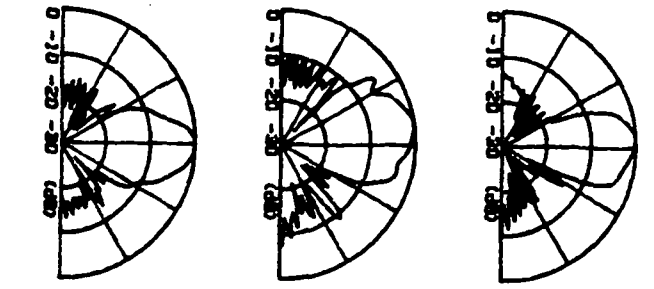

Bottom Center Top

3 mm

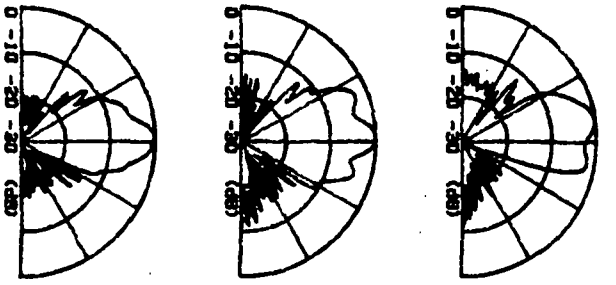

5 mm

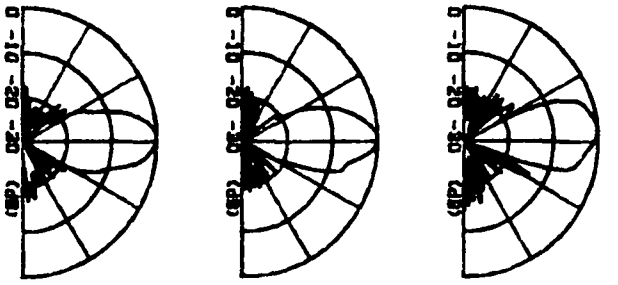

8 mm

(a)

Figure 2.7.

H–PLANE

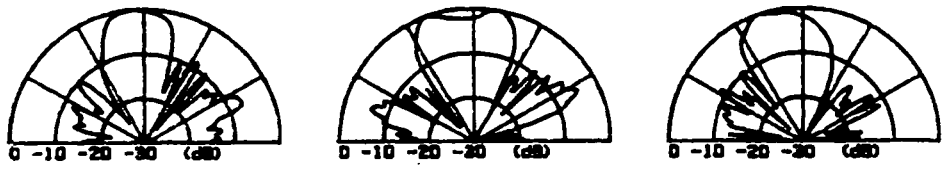

3 mm

Left Center Right

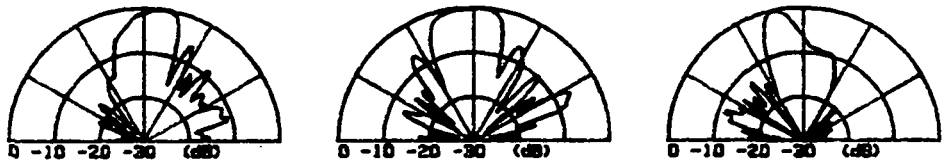

5 mm

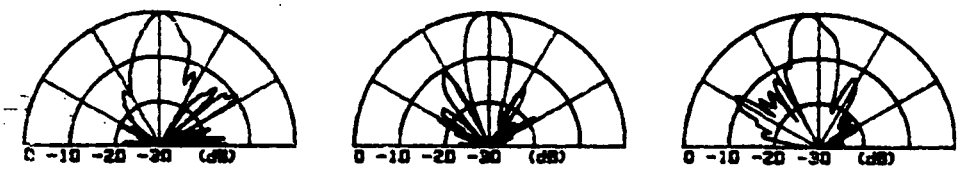

8 mm

(b)

Figure 2.7.

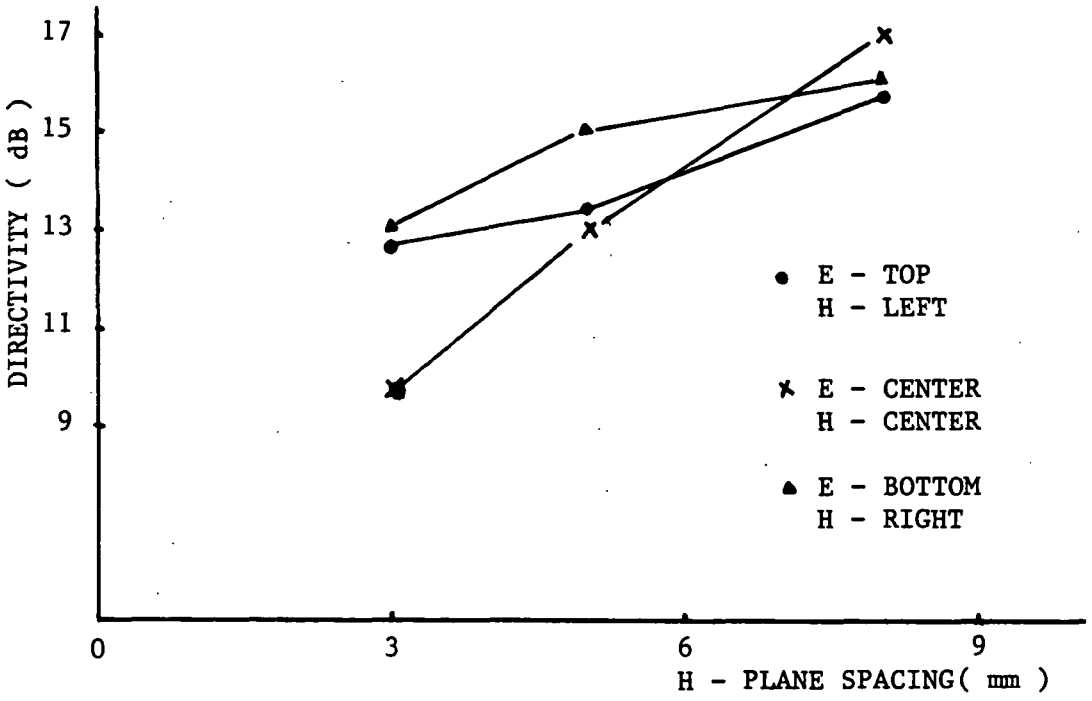
17
15
13
11
9
DIRECTIVITY (dB)
0
3
6
9
H - PLANE SPACING(mm)
E - TOP
H - LEFT
E - CENTER
H - CENTER
E - BOTTOM
H - RIGHT

Figure 2.8.

H–PLANE

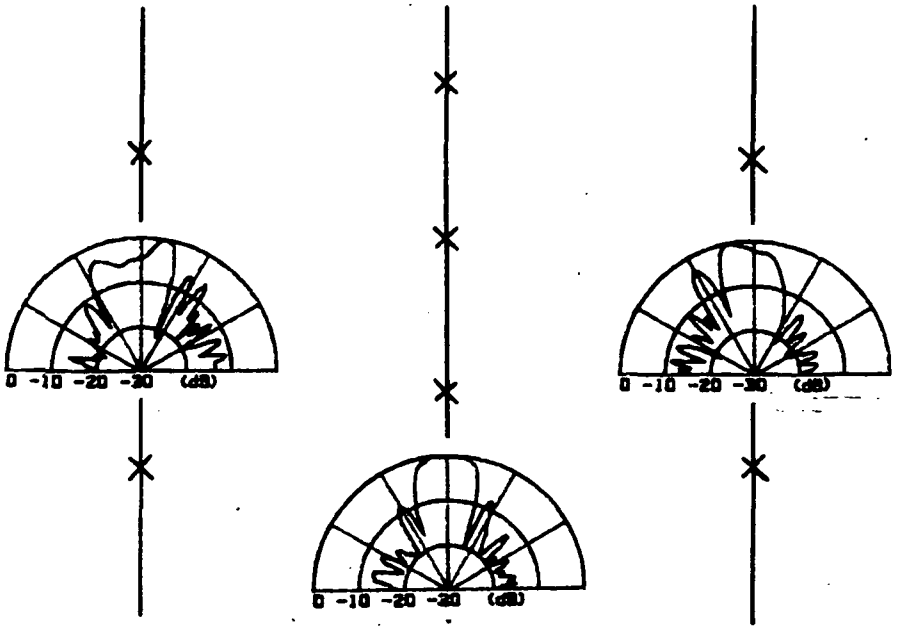

E–PLANE

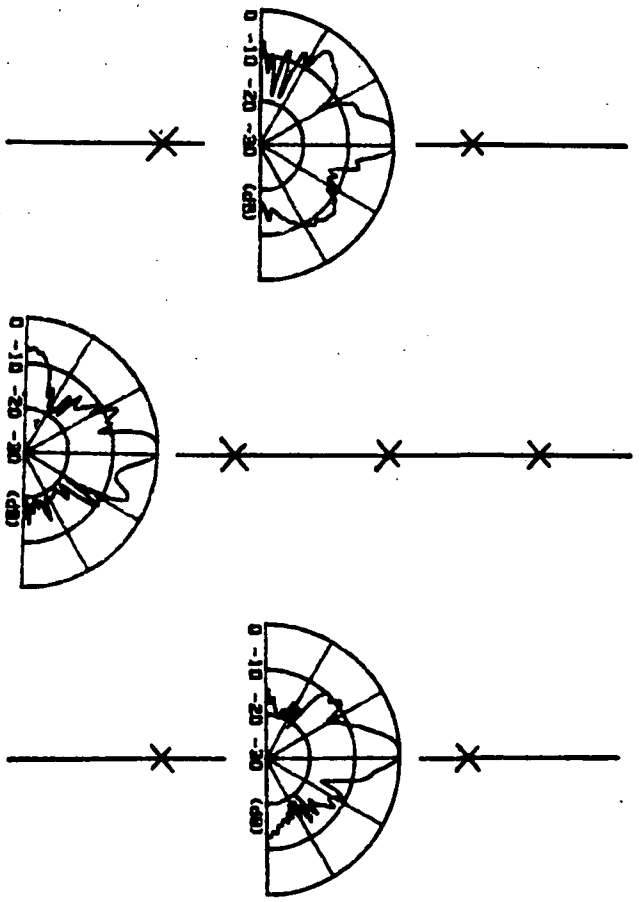

Figure 2.9.

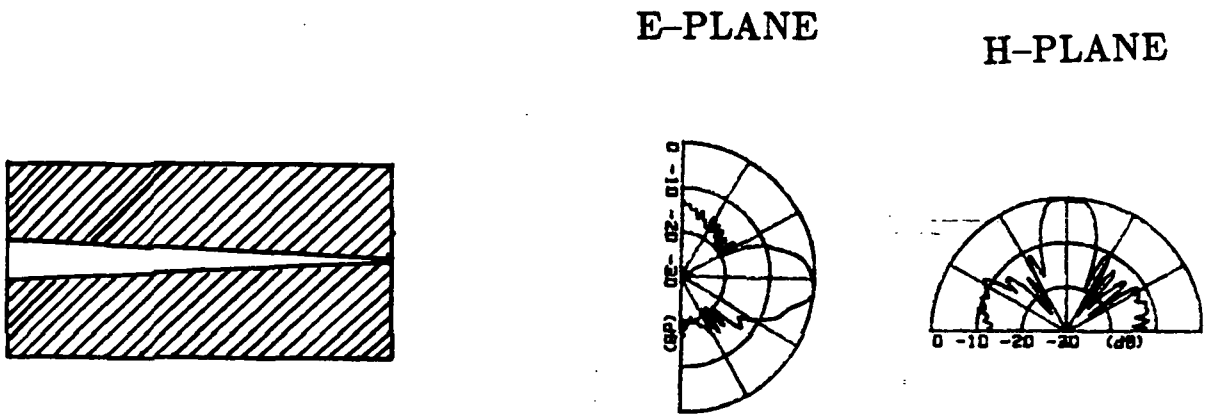

(a)

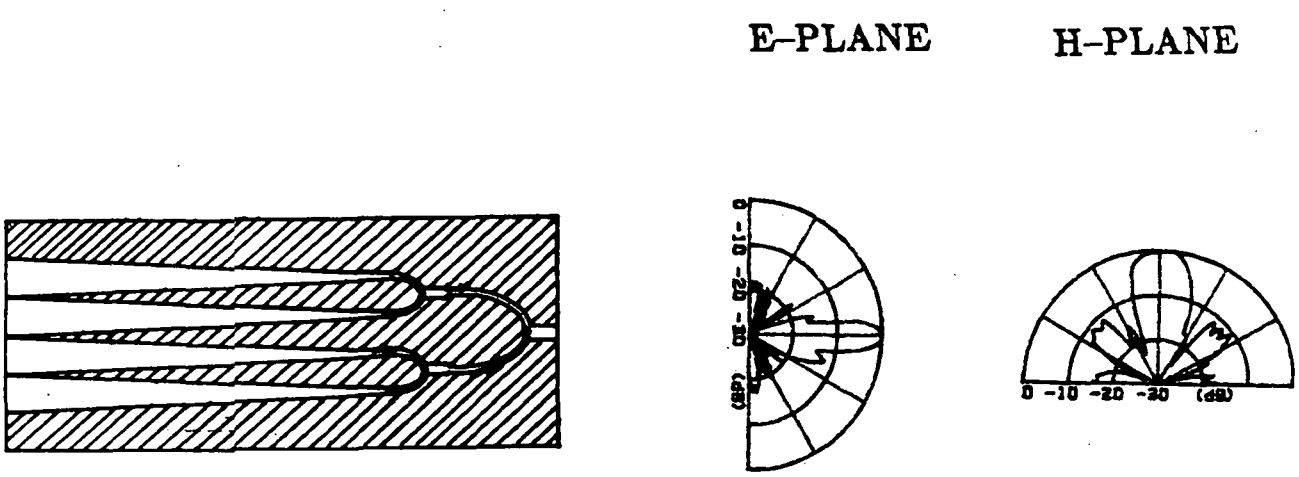

(b)

Figure 2.10

Appendix A

N86-30893

D2
15 P.
18338
MK149394

APPENDIX A

Characteristic Impedance of a Wide Slot Line on Low Permittivity Substrates*

R. Janaswamy, Student Member
D.H. Schaubert, Senior Member

Department of Electrical and Computer Engineering
University of Massachusetts
Amherst, MA 01003

July 1985

* This work was supported by NASA Langley Research Center under grant number NAG-1-279

Abstract: Computed results on the characteristic impedance of wide slots etched on an electrically thin substrate of low dielectric constant ε_r are presented. These results combined with those in [1] provide design data for these slotlines. Curves are presented for ε_r = 2.22, 3.0, 3.8 and 9.8. Comparison is shown for the characteristic impedance between the present calculations and those available in the literature for high-ε_r substrates. Empirical formulas, based on least square curve fitting, are presented for the normalized slot wavelength λ'/λ_o and the characteristic impedance Z_o over the range: $0.0015 \leq W/\lambda_o \leq 1.0$, $0.006 \leq d/\lambda_o \leq 0.06$, $2.22 \leq \varepsilon_r \leq 9.8$.

I. Introduction

Impedance properties of a slot line shown in Fig. 1 have been thoroughly treated in the literature by a number of authors [2,3]. All the previous work has been confined to slots on high-ε_r substrates ($\varepsilon_r \geq 9.6$), which are typically used for circuit applications. No data have been reported for slots on low-ε_r substrates, where slot lines have interesting applications as antennas [4-6]. Knowledge of the characteristic impedance of slot lines on these low-ε_r substrates is highly desirable in designing a proper feed and accompanying circuits for these antennas.

In this paper, computed data are presented for the characteristic impedance Z_o for slots on low-ε_r substrates. The problem is formulated in the spectral domain and the eigenvalue equation for the eigen pair (λ', e^s), where λ' is the slot wavelength and e^s the slot field, is solved by using the spectral Galerkin's method [7]. The slot characteristic impedance Z_o is calculated in the spectral domain from the slot field.

II. Formulation of the Problem and Numerical Results

The characteristic impedance Z_o of the slot line shown in Fig. 1 is defined as [2]

$$Z_o = \frac{|V_o|^2}{P_f} \tag{1}$$

where V_o is the voltage across the slot in the plane of the slot and is given in terms of the transverse electric field component E_x as

$$V_o = \int_{-W/2}^{W/2} E_x dx = \tilde{E}_x(\alpha)\Big|_{\alpha=0} = \tilde{E}_x(0) \tag{2}$$

'~' denotes quantities Fourier transformed with respect to the x-axis and α is the transform variable. P_f is the real part of the complex power flow (actually real in this case for a propagating mode) along the slot and is given by

$$\begin{aligned} P_f &= \int_x \int_{y \text{ plane}} (E_x H_y^* - E_y H_x^*)\, dxdy \\ &= \frac{1}{2\pi} \int_\alpha \int_{y \text{ plane}} (\tilde{E}_x \tilde{H}_y^* - \tilde{E}_y \tilde{H}_x^*)\, d\alpha dy \end{aligned} \tag{3}$$

where E_x, E_y, H_x, H_y are fields tangential to the z=constant plane. The second equality in (3) follows from Parseval's theorem and * denotes the complex conjugate.

The fields $\tilde{E}$ and $\tilde{H}$ in the spectral domain pertaining to the air and dielectric regions of the slot line can be related to the aperture field (i.e., field in the slot), which is modeled by the method of moments. As was done in [1], the field in the slot region is expanded as

$$\begin{aligned} E_x^s &= \sum_{n=0}^{M_x} a_n e_n^x \\ e_n^x &= \left(\frac{2}{\pi W}\right) \frac{T_{2n}\left(\frac{2x}{W}\right)}{\sqrt{1-\left(\frac{2x}{W}\right)^2}} \quad ; \; n = 0,1,\ldots \end{aligned} \tag{4}$$

$$E_z^s = \sum_{m=1}^{M_z} b_m e_m^z$$

$$e_m^z = \left(\frac{2}{\pi W}\right) \sqrt{1-\left(\frac{2x}{W}\right)^2}\, U_{2m-1}\left(\frac{2x}{W}\right) \quad ; \; m = 1,2,\ldots \tag{5}$$

where T_n and U_n are Tchebycheff polynomials of the I and II kind respectively.

The Fourier transforms of the above basis functions can be found readily in closed form as [8]

$$\tilde{e}_n^x = (-1)^n J_{2n}\left(\frac{\alpha W}{2}\right) \quad , \quad n = 0,1,\ldots \tag{6}$$

$$\tilde{e}_m^z = j(-1)^{m+1}\, 2m\, \frac{J_{2m}\left(\frac{\alpha W}{2}\right)}{\left(\frac{\alpha W}{2}\right)} \quad , \; m = 1,2,\ldots \tag{7}$$

The integration with respect to y in (3) can be done in closed form. However, the integration on the α variable must be done numerically. The slot wavelength λ' is stationary with respect to the slot field and it was found that λ' converges with only one basis function for the longitudinal field as reported in [1]. However, more than one basis function for E_z^s is needed for the convergence of the characteristic impedance Z_o for a wide slot. The maximum number of basis functions needed for E_x^s and E_z^s during the computation of Z_o was 5 and 3, respectively, when the slot width approached one free space wavelength λ_o.

Computer programs have been developed to compute λ' and Z_o for a specified ε_r, λ_o and d. As a check of these programs, Table 1 shows a comparison for Z_o between the present computations and those in [3]. Characteristic impedances for slot lines have been computed for $\varepsilon_r = 2.22$, 3.0, 3.8, 6.5 and 9.8 and for widths varying over $0.0015 \leq W/\lambda_o \leq 1.0$. Computed values of Z_o vs. W/λ_o with d/λ_o as a parameter are plotted in Figure 2.

Empirical formulas have been developed for the normalized slot wavelength λ'/λ_o and the slot characteristic impedance Z_o and are given in (8)-(15). These formulas have been obtained by least square curvefitting the computed data. In each case, the average of the absolute percentage error 'Av' and the maximum percentage error 'Max', observed in a systematic sample of 120 data points is given. Also, where possible, the region around which the maximum error has been observed is indicated.

The following formulas are all valid within $0.006 \leq d/\lambda_o \leq 0.060$.

$$2.22 \leq \varepsilon_r \leq 3.8$$

$$0.0015 \leq W/\lambda_o \leq 0.075$$

$$\lambda'/\lambda_o = 1.045 - 0.365\ell n\varepsilon_r + \frac{6.3(W/d)\varepsilon_r^{0.945}}{(238.64 + 100W/d)} - \left[0.148 - \frac{8.81(\varepsilon_r+0.95)}{100\varepsilon_r}\right] .\ell n(d/\lambda_o) \quad (8)$$

Av = 0.37%, Max = 2.2% (at one point)

$$Z_o = 60. + 3.69\sin\left[\frac{(\varepsilon_r-2.22)\pi}{2.36}\right] + 133.5\ell n(10\varepsilon_r)\sqrt{W/\lambda_o} + 2.81\left[1-0.011\varepsilon_r(4.48+\ell n\varepsilon_r)\right](W/d)\ell n(100d/\lambda_o) + 131.1(1.028-\ell n\varepsilon_r)\sqrt{d/\lambda_o} + 12.48(1+0.18\ell n\varepsilon_r)\frac{W/d}{\sqrt{\varepsilon_r -2.06+0.85(W/d)^2}} \quad (9)$$

Av = 0.67%, Max = 2.7% (at one point)

$$0.075 \leq W/\lambda_o \leq 1.0$$

$$\lambda'/\lambda_o = 1.194 - 0.24\ell n\varepsilon_r - \frac{0.621\varepsilon_r^{0.835}(W/\lambda_o)^{0.48}}{(1.344 + W/d)} - 0.0617\left[1.91 - \frac{(\varepsilon_r+2)}{\varepsilon_r}\right]\ell n(d/\lambda_o)$$

Av = 0.69%, Max = -2.6% (at two points, for $W/\lambda_o > 0.8$) (10)

$$Z_o = 133. + 10.34(\varepsilon_r-1.8)^2 + 2.87\left[2.96+(\varepsilon_r-1.582)^2\right]\left[\{W/d + 2.32\varepsilon_r - 0.56\}.\right.$$
$$\left.\{(32.5 - 6.67\varepsilon_r)(100d/\lambda_o)^2 - 1\}\right]^{\frac{1}{2}} - (684.45d/\lambda_o)(\varepsilon_r+1.35)^2$$
$$+ 13.23\left[(\varepsilon_r-1.722)W/\lambda_o\right]^2 \quad (11)$$

Av = 1.9%, |Max| = 5.4% (at three points, for $W/\lambda_o > 0.8$)

$$3.8 \leq \varepsilon_r \leq 9.8$$

$$0.0015 \leq W/\lambda_o \leq 0.075$$

$$\lambda'/\lambda_o = 0.9217 - 0.277\ell n\varepsilon_r + 0.0322(W/d)\left[\frac{\varepsilon_r}{(W/d+0.435)}\right]^{\frac{1}{2}} -$$
$$- 0.01\ell n(d/\lambda_o)\left[4.6 - \frac{3.65}{\varepsilon_r^2\sqrt{W/\lambda_o}(9.06-100W/\lambda_o)}\right] \quad (12)$$

Av = 0.6%, |Max| = 3% (at three points, occurs for $W/d > 1$ and $\varepsilon_r > 6.0$)

$$Z_o = 73.6 - 2.15\varepsilon_r + (638.9-31.37\varepsilon_r)(W/\lambda_o)^{0.6} + (36.23\sqrt{\varepsilon_r^2 + 41} - 225).$$
$$\frac{W/d}{(W/d+0.876\varepsilon_r-2)} + 0.51(\varepsilon_r+2.12)(W/d)\ell n(100d/\lambda_o) - 0.753\varepsilon_r(d/\lambda_o)/\sqrt{W/\lambda_o} \quad (13)$$

Av = 1.58%, Max = 5.4% (at three points, occurs for $W/d > 1.67$)

$$0.075 \leq W/\lambda_o \leq 1.0$$

$$\lambda'/\lambda_o = 1.05 - 0.04\varepsilon_r + 1.411\times10^{-2}(\varepsilon_r-1.421)\ell n\{W/d - 2.012(1-0.146\varepsilon_r)\}$$
$$+ 0.111(1-0.366\varepsilon_r)\sqrt{W/\lambda_o} + 0.139\{1+0.52\varepsilon_r\ell n(14.7-\varepsilon_r)\}(d/\lambda_o)\ell n(d/\lambda_o) \quad (14)$$

Av = 0.75%, |Max| = 3.2% (at two points, occurs for $W/\lambda_o = 0.075$, $d/\lambda_o > 0.03$)

$$Z_o = 120.75 - 3.74\varepsilon_r + 50[\tan^{-1}(2\varepsilon_r) - 0.8](W/d)^{\left[1.11 + \frac{0.132(\varepsilon_r-27.7)}{(100d/\lambda_o+5)}\right]} \cdot$$

$$\ell n[100d/\lambda_o + \sqrt{(100d/\lambda_o)^2+1}\ ] + 14.21(1-0.458\varepsilon_r)(100d/\lambda_o + 5.1\ell n\varepsilon_r - 13.1)$$

$$\cdot(W/\lambda_o+0.33)^2 \qquad (15)$$

Av = 2.0%, |Max| = 5.8% (at two points, occurs for $W/\lambda_o < 0.1$)

In the above formula, $\tan^{-1}(.)$ assumes its principal value.

III. Conclusion

A spectral domain Galerkin method is used to compute the characteristic impedance of wide slot lines on low ε_r substrates. Empirical formulas have been presented for the slot wavelength and the characteristic impedance over a wide range of slot widths. The data presented here supplement data already available on high ε_r substrates.

References

[1] R. Janaswamy and D.H. Schaubert, "Dispersion Characteristics for Wide Slot Lines on Low Permittivity Substrates," IEEE Trans. Microwave Theory and Tech., Vol. MTT-33, No. 8, pp. 723-726, August 1985.

[2] J.B. Knorr and K. Kuchler, "Analysis of Coupled Slots and Coplanar Strips on Dielectric Substrate," IEEE Trans. Microwave Theory and Tech., Vol. MTT-23, No. 7, pp. 541-548, July 1975.

[3] E.A. Mariani et al., "Slotline Characteristics," IEEE Trans. Microwave Theory and Tech., Vol. MTT-17, No. 12, pp. 1091-1096, December 1969.

[4] E.L. Kollberg et al., "New Results on Tapered Slot Endfire Antennas on Dielectric Substrate," presented at the 8th IEEE International Conference on Infrared and Millimeter Waves, Miami, December 1983.

[5] S.N Prasad and S. Mahapatra, "A New MIC Slot Line Aerial," IEEE Trans. Antennas and Propagat., Vol. AP-31, No. 3, pp. 525-527, May 1983.

[6] J.F. Johansson, "Investigation of Some Slotline Antennas," M.S. Thesis, Chalmers University, Gothenberg, Sweden, 1983.

[7] T. Itoh and R. Mittra, "Dispersion Characteristics of Slot Lines," Electron Lett., Vol. 7, pp. 364-365, July 1971.

[8] A. Erdelyi et al., Tables of Integral Transforms, Vol. 2, McGraw Hill Book Co., New York, 1954.

Figures

Figure 1. Geometry of slot line.

Figure 2. Characteristic impedance of slot line as a function of normalized slot width. a) $\varepsilon_r = 2.22$ b) $\varepsilon_r = 3.0$ c) $\varepsilon_r = 3.8$ d) $\varepsilon_r = 9.8$.

Table 1. Comparison of calculated slot characteristic impedance Z_o.

Table 1

Comparison of calculated slot characteristic impedance Z_o.

ϵ_r	d/λ_o	W/d	$Z_o(\Omega)$	
			From curves in [3]	Present
9.6	0.06	1.0	140	142
11.0	0.04	1.5	160	160
13.0	0.03	0.4	80	82
16.0	0.025	2.0	150	151
20.0	0.03	1.0	100	101

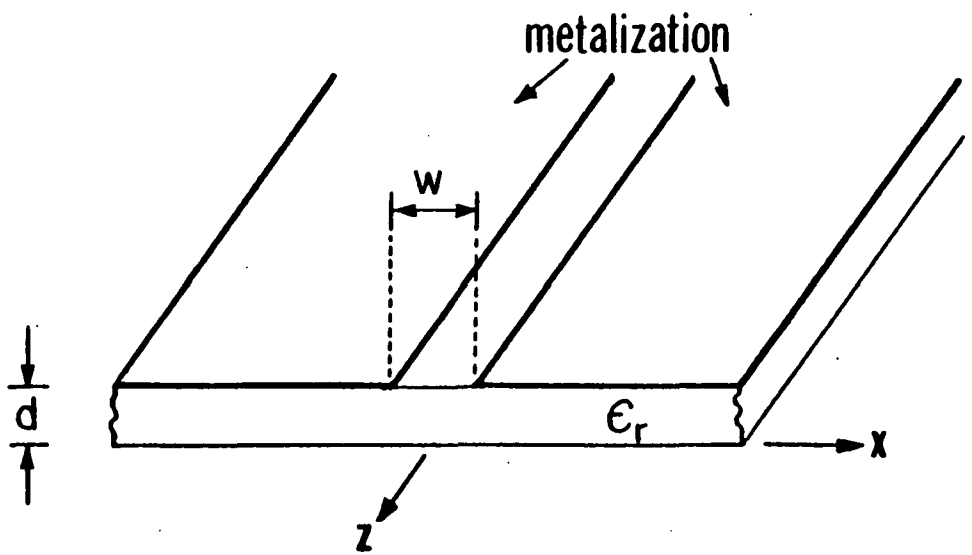

Fig. 1

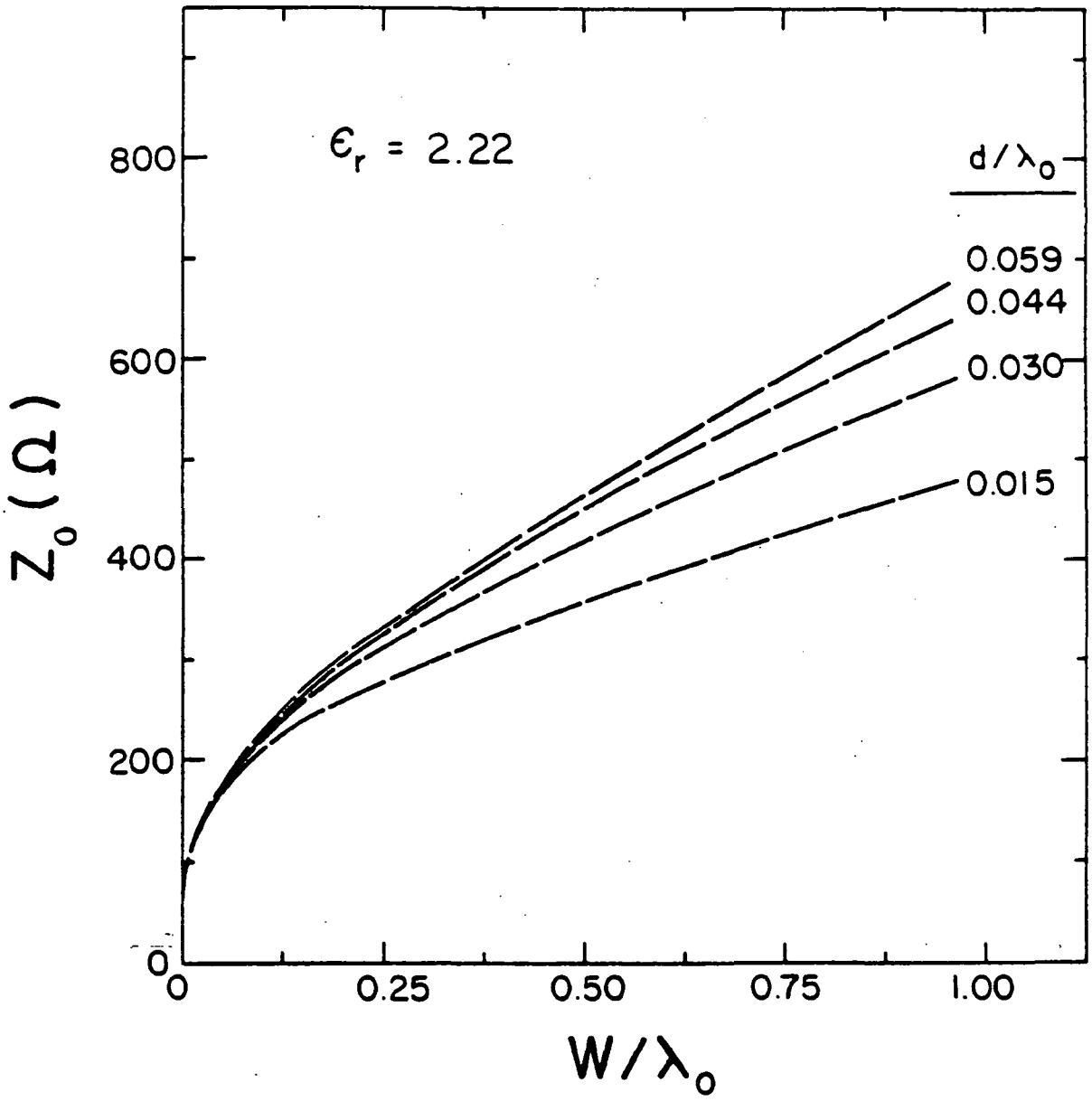
ϵ_r = 2.22
d/λ_0
0.059
0.044
0.030
0.015
800
600
400
200
0
0
0.25
0.50
0.75
1.00
Z_0 (Ω)
W/λ_0

Fig. 2a

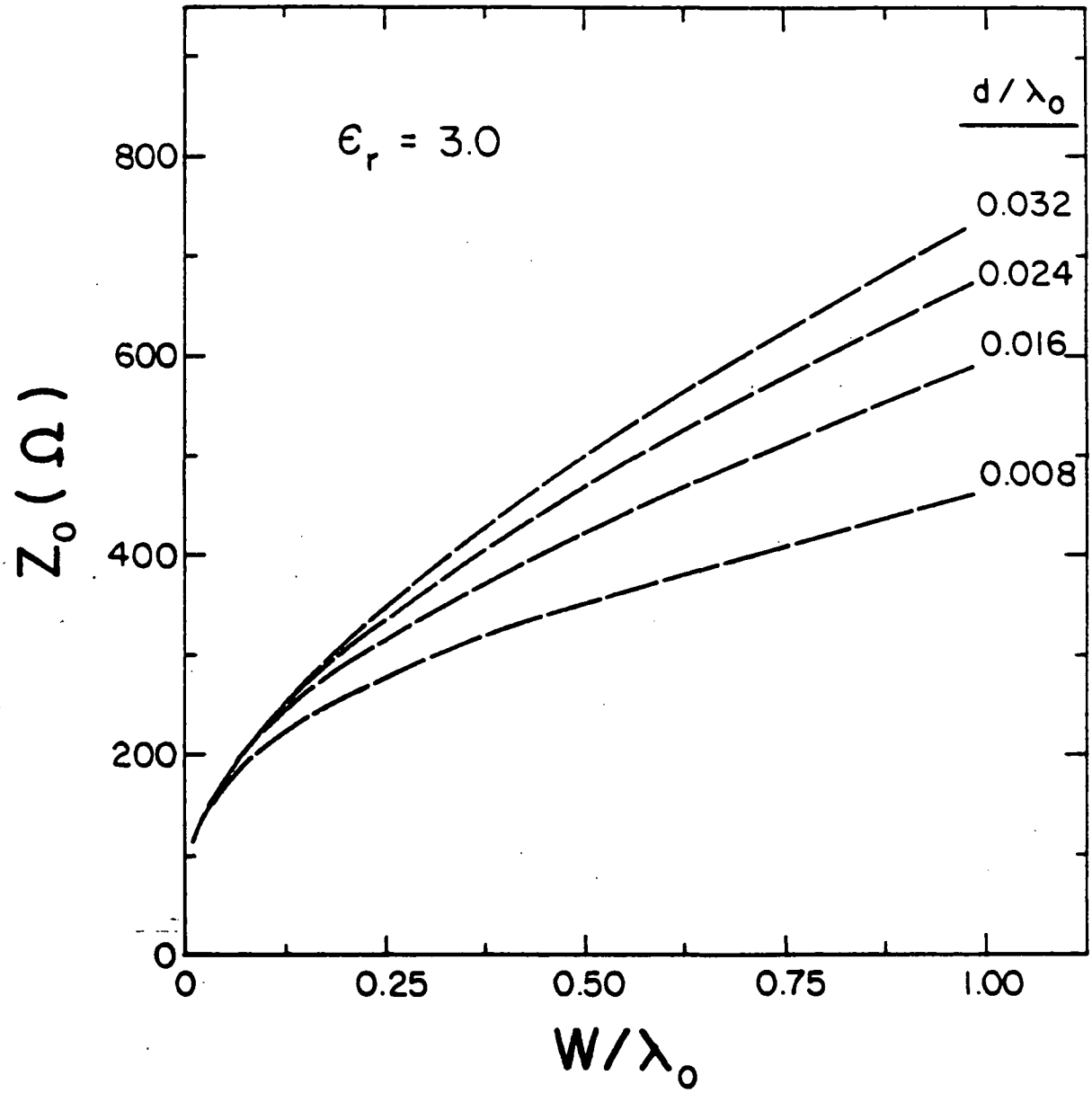
ϵ_r = 3.0
d / λ0
0.032
0.024
0.016
0.008
800
600
400
200
0
Z0 (Ω)
0
0.25
0.50
0.75
1.00
W/λ0

Fig. 2b

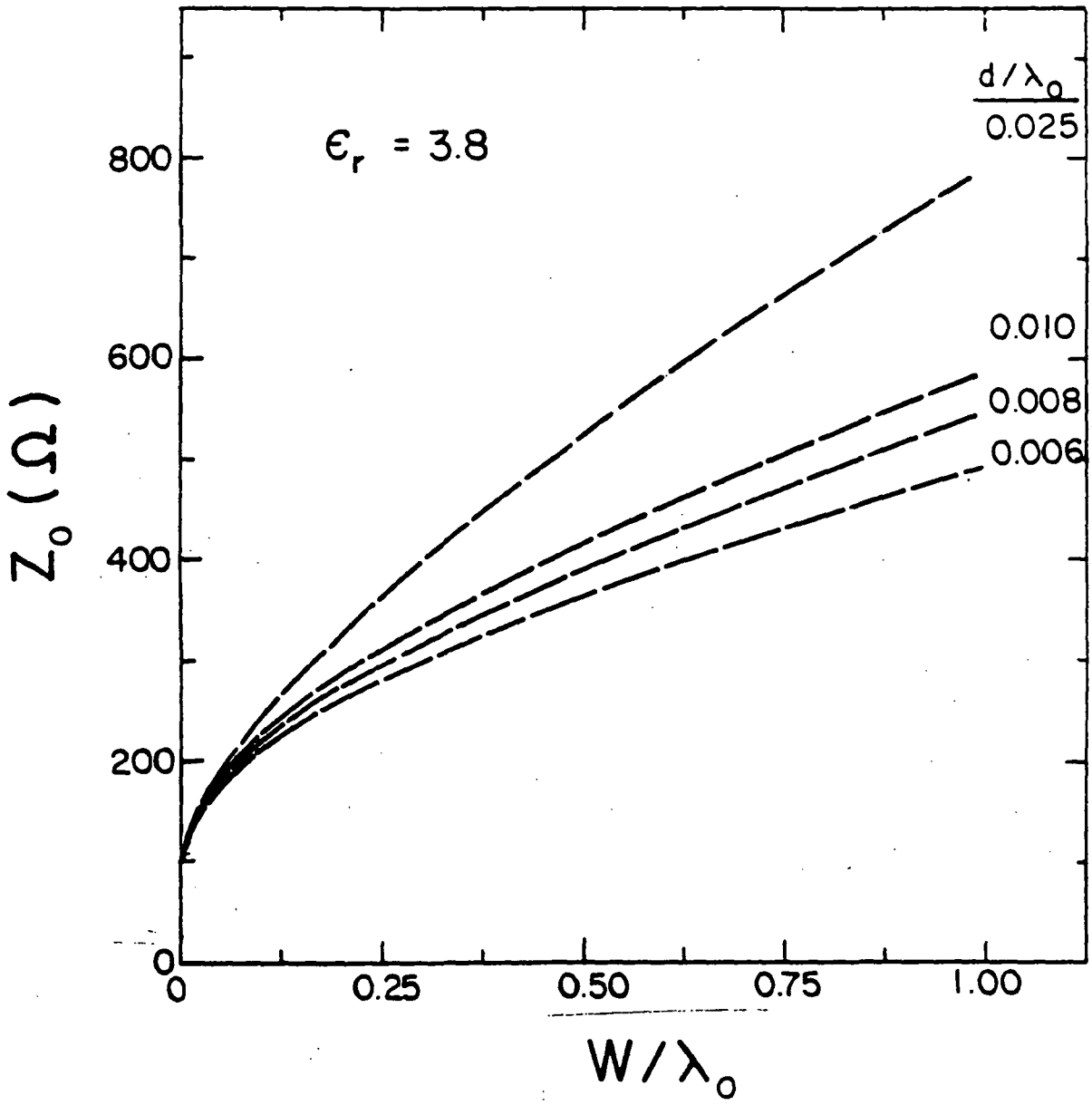
ϵ_r = 3.8
d/λ_0
0.025
0.010
0.008
0.006
800
600
400
200
0
Z_0 (Ω)
0
0.25
0.50
0.75
1.00
W/λ_0

Fig. 2c

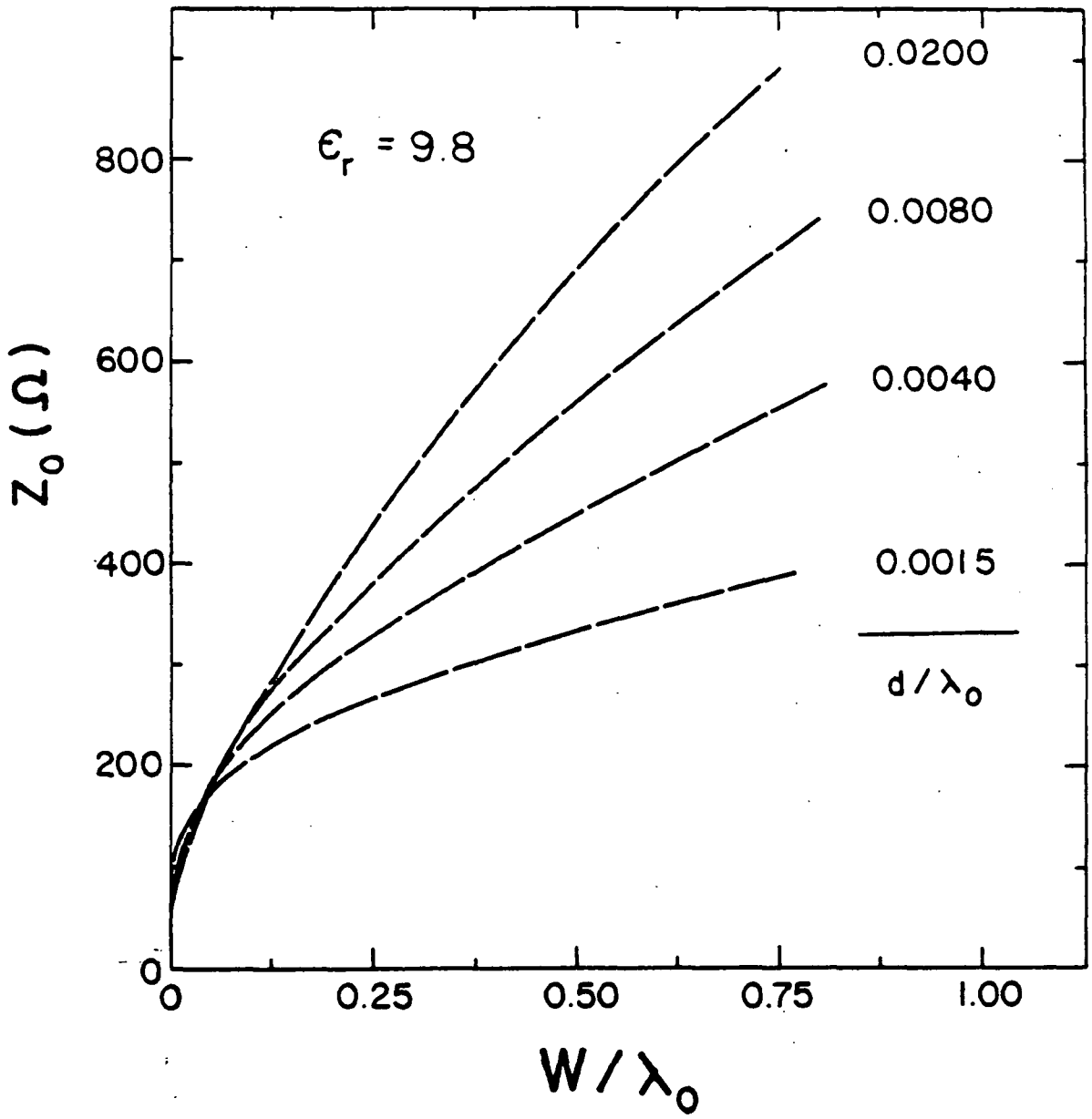
$\epsilon_r = 9.8$
0.0200
0.0080
0.0040
0.0015
d/λ_0
$Z_0\,(\Omega)$
800
600
400
200
0
0
0.25
0.50
0.75
1.00
W/λ_0

Fig. 2d